RE-426J

NONLINEAR BEHAVIOR OF SHELLS OF REVOLUTION UNDER CYCLIC LOADING

April 1972

RESEARCH DEPARTMENT

GRUMMAN AEROSPACE CORPORATION
BETHPAGE NEW YORK

Grumman Research Department Report RE-426J

NONLINEAR BEHAVIOR OF SHELLS OF REVOLUTION UNDER CYCLIC LOADING[†]

by

H. S. Levine, H. Armen, Jr.,
R. Winter, and A. Pifko

Materials and Structural Mechanics

April 1972

[†]Presented at the National Symposium on Computerized Structural Analysis and Design, Washington, D.C., March 27-29, 1972

Approved by: Charles E. Mack, Jr.
Charles E. Mack, Jr.
Director of Research

NONLINEAR BEHAVIOR OF SHELLS OF REVOLUTION UNDER CYCLIC LOADING[†]

by

Howard S. Levine
Research Scientist

Harry Armen, Jr.
Research Scientist

Robert Winter
Research Engineer

Allan Pifko
Research Engineer

Grumman Aerospace Corporation
Research Department, Plant 35
Bethpage, New York 11714

Abstract

A large-deflection elastic-plastic analysis is presented, applicable to orthotropic axisymmetric plates and shells of revolution subjected to monotonic and cyclic loading conditions. The analysis is based on the finite-element method. It employs a new higher order, fully compatible, doubly curved orthotropic shell-of-revolution element using cubic Hermitian expansions for both meridional and normal displacements. Both perfectly plastic and strain hardening behavior are considered. Strain hardening is incorporated through use of the Prager-Ziegler kinematic hardening theory, which predicts an ideal Bauschinger effect. Numerous sample problems involving monotonic

[†]This research is partially supported by NASA/Langley Research Center under Contract NAS 1-10087.

and cyclic loading conditions are analyzed. The monotonic results are compared with other theoretical solutions. Experimental verification of the accuracy of the analysis is also provided by comparison with results obtained from a series of tests for centrally monotonically-loaded circular plates that are simply supported at their edges.

NONLINEAR BEHAVIOR OF SHELLS OF REVOLUTION UNDER CYCLIC LOADING[†]

by

Howard S. Levine
Research Scientist

Harry Armen, Jr.
Research Scientist

Robert Winter
Research Engineer

Allan Pifko
Research Engineer

Grumman Aerospace Corporation
Research Department, Plant 35
Bethpage, New York 11714

I. Introduction

The need for a capability of determining the reserve strength of shell structures accurately and predicting their failure loads under a variety of realistic loading conditions has stimulated substantial efforts toward developing methods for the nonlinear analysis of these structures. For shells of revolution, effects resulting from both geometric [1-3] and material nonlinearities [4-6] have been considered separately, and in several instances the simultaneous effects of both types of nonlinearity have been treated [7-9]. In general, these studies have been concerned solely with

[†]This research is partially supported by NASA/Langley Research Center under Contract NAS 1-10087.

monotonic loading conditions, and the effect of material nonlinearity is accounted for starting at a load level corresponding to the elastic limit and up to a maximum specified load, or until structural failure occurs. Only in rare instances have unloading and reversed loading been considered [10,11].

In the present paper, a large-deflection, elastic-plastic analysis is presented, applicable to orthotropic axisymmetric plates and shells of revolution subjected to monotonic and cyclic loading conditions. The theoretical work is based on the stiffness method of finite-element analysis in conjunction with the concept of initial strains, material nonlinearity being introduced by interpreting plastic strains as initial strains. Large-deflection effects are included via an incremental Eulerian approach, and the results are valid for moderate rotations and small strains. Both strain hardening and perfectly plastic material behavior are considered. Strain hardening is represented by using the Prager-Ziegler [12,13] kinematic hardening theory, so that the Bauschinger effect is accounted for.

A new higher order, fully compatible, doubly curved, orthotropic shell-of-revolution element [14] employing cubic

Hermitian expansions for both meridional and normal displacements has been developed and used to obtain the results presented. Verification of the accuracy of the analysis has been accomplished by comparison with previously obtained numerical results.

An experimental program was initiated to gain further insight into the complex response associated with both types of nonlinearities and to provide further verification of the numerical solutions. Toward these ends, a series of experiments were performed on centrally loaded, simply supported, circular plates. Agreement between data obtained from these experiments and the present analysis ranges from good to excellent for cases thus far restricted to monotonic loading.

II. Development of Governing Matrix Equations

The method employed in the present paper uses an incremental formulation for the large-deflection, elasto-plastic problem and is based on a variational principle presented in Ref. 15. The approach used here is identical in concept to that outlined in Ref. 8, with the exception that plasticity is treated by means of the initial strain concept [16,17] in the present work, whereas the tangent modulus method [18] is used in Ref. 8.

As the initial step towards the development of the governing matrix equation, we choose a reference state, Γ_R, in the body, for which the states of stress, strain, and deformation are known. We now choose the next state to be incrementally adjacent to the initial state with all quantities referred to the reference state, i.e., $x_i = X_i + \Delta u_i$, where x_i are the new coordinates of an arbitrary point, X_i are the original coordinates in the local coordinate system, and Δu_i are the incremental deflections of the point in going from the reference state to the current state [15].

At the start of a load increment, let the stresses, surface tractions, and body forces acting on the structure be denoted by S_{ij}, $T_i^{(0)}$, and $F_i^{(0)}$. These quantities are referred to a unit of "undeformed" area, i.e., before the addition of the current load increment. They take into account the effects of any previous initial strains present in the body. The application of an incremental load to the body, expressed in terms of ΔT_i and ΔF_i, result in additional stresses $\Delta\sigma_{ij}$, displacements Δu_i, plastic (initial) strains $\Delta\epsilon_{ij}^p$, and the distortion of the body to its new configuration given by x_i.

The total stresses, surface tractions, and body forces, referred to the unit undeformed area and in the new coordinate directions x_i, are

$$\sigma_{ij} = S_{ij} + \Delta\sigma_{ij}$$

$$F_i = F_i^{(0)} + \Delta F_i \qquad (1)$$

$$T_i = T_i^{(0)} + \Delta T_i \quad .$$

The development of the governing matrix equation may be approached by one of several alternative procedures. The authors choose here the principle of virtual work, which, for an incremental method, may be written as [15]:

$$\int_V (S_{ij} + \Delta\sigma_{ij})\delta(\Delta\epsilon_{ij})dV = \int_S (T_i^{(0)} + \Delta T_i)\delta(\Delta u_i)dS + \int_V (F_i^{(0)} + \Delta F_i)\delta(\Delta u_i)dV \quad . \qquad (2)$$

Here $\Delta\epsilon_{ij}$ is Green's strain tensor that refers to the original or "undeformed" volume of the element

$$\Delta\epsilon_{ij} = \Delta e_{ij} + \Delta\eta_{ij} \quad . \qquad (3)$$

In this expression Δe_{ij} are the terms that yield a linear strain-displacement relationship, while $\Delta\eta_{ij}$ are those associated with the nonlinear terms in the strain-displacement relationship. The incremental constitutive equations are taken to be in the following form

$$\Delta\sigma_{ij} = E_{ijkl}(\Delta\epsilon_{kl} - \Delta\epsilon^{p}_{kl}) \quad , \tag{4}$$

where $\Delta\epsilon^{p}_{kl}$ are the initial or plastic strains developed in the current increment based upon the "undeformed" geometry. These are assumed to be small and independent of the total strains. The terms, E_{ijkl}, are the linearly elastic material properties.

Substituting the stress-strain relations, Eqs. (4) and (3) into Eq. (2) yields

$$\begin{aligned}
\int_V \left[\Delta e_{ij} E_{ijkl} \delta(\Delta e_{kl}) + S_{ij}\delta(\Delta\eta_{ij})\right] dV = \\
\int_S \Delta T_i \delta(\Delta u_i) dS + \int_V \Delta F_i \delta(\Delta u_i) dV \\
+ \int_V \Delta\epsilon^{p}_{ij}\, E_{ijkl}\delta(\Delta e_{kl}) dV - \left(\int_V S_{ij}\delta(\Delta e_{ij}) dV\right. \\
\left. - \int_S T^{(0)}_i \delta(\Delta u_i) dS - \int_V F^{(0)}_i \delta(\Delta u_i) dV\right) \\
- \left(\int_V \Delta\eta_{ij} E_{ijkl}\, \delta(\Delta e_{kl}) dV + \int_V \Delta\sigma_{ij}\, \delta(\Delta\eta_{ij}) dV\right)
\end{aligned} \tag{5}$$

We now have an equation that is similar in form to that presented in Ref. 8, with the exception of those terms associated with initial strains. As in Ref. 8, it is assumed that, although total strains may be large, incremental strains are small, and thus the last two terms of Eq. (5) (which are cubic and quartic in displacement increments) may be neglected when compared to terms that are quadratic in displacement increments. These terms that are neglected lead to the matrices $[N_1]$ and $[N_2]$ of Ref. 19 and must be retained in a total Lagrangian formulation. An additional matrix due to the presence of initial strains is also generated from the last term of Eq. (5), but since it contributes terms of the same order of magnitude as the other term neglected, it too need not be retained.

We then have

$$\int_V \left[S_{ij}\delta(\Delta\eta_{ij}) + \Delta e_{kl}\, E_{ijkl}\delta(\Delta e_{ij}) \right] dV =$$

$$\int_S \Delta T_i \delta(\Delta u_i) dS + \int_V \Delta F_i \delta(\Delta u_i) dV$$

$$+ \int_V \Delta\epsilon^p_{ij}\, E_{ijkl}\delta(\Delta e_{kl}) dV \tag{6}$$

$$+ \left(\int_S T^{(0)}_i \delta(\Delta u_i) dS + \int_V F^{(0)}_i \delta(\Delta u_i) dV - \int_V S_{ij}\delta(\Delta e_{ij}) dV \right) .$$

If the initial stress state, S_{ij}, $T^{(0)}_i$, and $F^{(0)}_i$, is in equilibrium at the start of the incremental step, then the last three terms of Eq. (6) vanish and we get the standard incremental initial-strain large-deflection formulation:

$$\int_V \left[S_{ij}\delta(\Delta\eta_{ij}) + \Delta e_{kl} E_{ijkl}\delta(\Delta e_{ij}) \right] dV = \int_S \Delta T_i \delta(\Delta u_i) dS$$

$$+ \int_V \Delta F_i \delta(\Delta u_i) dV + \int_V \Delta\epsilon^p_{ij} E_{ijkl}\delta(\Delta e_{kl}) dV \tag{7}$$

The first term of this equation yields the initial stress stiffness matrix after the rotations (or other nonlinear terms)

have been expressed in terms of nodal degrees of freedom. The second term leads to the conventional stiffness matrix. The first two terms on the right side lead to the consistent load vectors for surface tractions and body forces, respectively. The last term on the right side leads to the initial-strain stiffness matrix which is multiplied by a vector of plastic (initial) strains to be used as an "effective" plastic load vector.

Because we use a predictor procedure, however, the initial stress state may not be in equilibrium before the current load step. The results for the next step may be adjusted or corrected for this imbalance by introducing a residual force given by [8]

$$R_i = \int_S T_i^{(0)} \delta(\Delta u_i) dS + \int_V F_i^{(0)} \delta(\Delta u_i) dV - \int_V S_{ij} \delta(\Delta e_{ij}) dV \quad . \tag{8}$$

Any discrepancies due to the neglect of the change in direction of the load are also accounted for in Eq. (8), since the total load is applied to the structure in its current configuration. The total stresses σ_{ij} obtained at the end of load increment N become the initial stresses for step $(N + 1)$. These must now be related to the new deformed area (which is the undeformed area for step $N + 1$). The

transformation that accomplishes this is presented in Ref. 8 and written here as

$$S_{ij} = (1 - \Delta e_{kk})\sigma_{ij} + (\Delta e_{jk} + \Delta\omega_{jk})\sigma_{ik} + (\Delta e_{ik} + \omega_{ik})\sigma_{jk} , \qquad (9)$$

where the $\Delta\omega_{ik}$ are the incremental rotations. Similar transformations must be carried out for the surface tractions, body forces, and initial strains.

We will, at this point, mention that the last two terms of Eq. (5) need not be neglected and can be included without the formation of any additional stiffness matrices besides the required initial stress stiffness matrix and initial-strain stiffness matrix. These terms may be retained in a predictor process in which values for $\Delta\sigma_{ij}$ and $\Delta\eta_{ij}$ obtained from the previous step (appropriately extrapolated) are used in the formulation of the appropriate stiffness matrices for the next incremental step. This should permit the use of larger step sizes in the current formulation. This latter concept was not used to obtain the results presented here.

III. Final Matrix Equations and Solution Procedures

The final form of the incremental equations used in the finite-element formulation is obtained from Eq. (6). The

displacements $\{\Delta u\}$, linear total strains $\{\Delta e_{ij}\}$, and rotations $\{\Delta\omega_{ij}\}$ are related to the nodal generalized displacements $\{\Delta u_i\}$ via the following matrix relations:

$$\begin{aligned} \{\Delta u\} &= [N]\{\Delta u_i\} \\ \{\Delta e_{ij}\} &= [W]\{\Delta u_i\} \\ \{\Delta\omega_{ij}\} &= [\Omega]\{\Delta u_i\} \quad . \end{aligned} \tag{10}$$

We then have

$$\left([k^{(0)}] + [k^{(1)}]\right)\{\Delta u_i\} = \{\Delta P_i\} + \{\Delta Q_i\} + \{R_i\} \tag{11}$$

where

$$[k^{(0)}] = \int_V [W]^T[E][W]dV$$

$$[k^{(1)}] = \int_V [\Omega]^T[S_{ij}][\Omega]dV$$

$$\{\Delta P_i\} = \int_S [N]^T\{\Delta T^{(0)}\}dS$$

$$\{\Delta Q_i\} = \int_V [W]^T[E]\{\Delta\epsilon^P\}dV$$

$$\{R_i\} = \int_S [N]^T \{T^{(0)}\} dS - \int_V [W]^T \{S_{ij}\} dV$$

and body force terms have been neglected, since they are not considered in this paper. Here $[k^{(0)}]$ is the conventional stiffness matrix, $[k^{(1)}]$ is the "initial stress" or geometric stiffness matrix, $\{\Delta P_i\}$ is the vector of applied loads, $\{\Delta Q_i\}$ is the effective plastic load vector, and $\{R_i\}$ is the vector of residual forces due to the existence of any equilibrium imbalance that may exist because of the predictor nature of the numerical solution procedure.

The specific forms of the matrices used in the present analysis for the shell element are presented in the Appendix. For the small-deflection analysis the procedure followed is to calculate the value of the load at which plastic deformation first occurs and is based upon an elastic analysis and application of a yield criterion. From this point, the load is then incremented to a maximum value, with new increments of displacement, plastic strain, and stress calculated at each step and total values obtained by summing incremental values. The plastic strain increments used in the plastic load vector are those calculated from the previous step. Since this is a small-deflection analysis, the stiffness

matrix need never be reformed. The residual force vector was not used in any of the small-deflection problems. At the maximum load, a new critical load for which yielding begins in the reverse direction is calculated, based upon elastic unloading to this point. Procedures for determining this load are presented in Refs. 20,21. This critical load may occur before all the load is removed from the structure because of the presence of residual stress and the existence of the Bauschinger effect. At this new critical value, the load is then incremented to the new specified maximum (minimum) value, and then this procedure is repeated for as many half cycles as desired.

For the large-deflection elastic-plastic analysis, the load is applied in small increments from the initial unloaded state. At the end of each increment, new increments of deflection, stress, strain, and plastic strain are calculated. Total quantities, such as the initial stresses S_{ij}, are calculated by using appropriate transformations, and the geometry of the structure is updated. Again the plastic strain increments used are those calculated in the previous step. The total stiffness matrix is reformed at every increment, together with the incremental load vector, plastic load vector,

and residual load vector. The element contributions are then assembled and the system of linear incremental equations is again solved and the process repeated until the maximum specified load is reached or structural failure occurs. If the response to cyclic loads is desired, the load increment is reversed at the maximum load, and the incremental process is repeated until the new maximum (minimum) load is reached. This procedure is then repeated for as many load cycles as desired.

For the large-deflection problem the most time-consuming feature is the reassembly of the stiffness matrix and solution of the linear incremental equations. It becomes convenient, therefore, to consider the possibility of treating the large-deflection terms as well as the plasticity effects as effective loads. This may be done by rewriting Eq. (11) as

$$[k^{(0)}]\{\Delta u_i\} = -[k^{(1)}]\{\Delta u_i\}^{N-1} + \{\Delta P_i\} + \{\Delta Q_i\} + \{R_i\}, \quad (12)$$

where now the product of the initial-stress stiffness matrix and the vector of displacement increments of the previous step is treated as an "effective geometric load." The stiffness matrix $[k^{(0)}]$ may be re-formed every M steps ($M \geq 1$),

with the possibility of saving a considerable amount of time. However, it is conjectured that the use of this solution procedure may lead to numerical instabilities, although none were observed in the limited number of problems solved by the authors. The use of the geometric terms as effective loads is not new, and has been used in many Lagrangian formulations with great success [22].

IV. Plasticity Relations

Appropriate plasticity relations to determine values of stress and plastic strain developed during each increment are now considered. Hill's yield criterion [23] for an orthotropic material, which reduces to the Von Mises yield condition for isotropic materials, is used to predict initial yield and to obtain the flow rules of plasticity. The capability of handling both strain hardening and ideally plastic behavior is included in the analysis. While orthotropic behavior is included in the case of ideal plasticity, only isotropic behavior is now allowed when the material strain hardens. There are several theories to treat the plastic behavior of strain hardening orthotropic materials, but the acceptance of a suitable one awaits further experimental verification.

We may write the increment of total strain as the sum of elastic and plastic strain increments:

$$\{\Delta\epsilon\} = \{\Delta\epsilon^e\} + \{\Delta\epsilon^p\} \quad . \tag{13}$$

The increment of elastic strain is related to the increment of stress through the matrix $[E]^{-1}$,

$$\{\Delta\epsilon^e\} = [E]^{-1}\{\Delta\sigma\} \quad . \tag{14}$$

For an elastic strain hardening material the plastic strain increments may be linearly related to the stress increments through a matrix $[C]$, as follows

$$\{\Delta\epsilon^p\} = [C]\{\Delta\sigma\} \quad . \tag{15}$$

The elements of this matrix are determined by choosing an appropriate hardening theory. The kinematic hardening theory is used for all problems presented in this paper. The elements of the matrix $[C]$ for plane stress, obtained by using Drucker's postulate [24] in conjunction with the Prager-Ziegler kinematic hardening theory [12,13], are presented in Refs. 20 and 21. Both linear and nonlinear hardening behavior can be represented. For the nonlinear behavior, a Ramberg-Osgood representation [25] of the stress-strain law is employed.

Using the expressions for $\{\Delta\epsilon^e\}$ and $\{\Delta\epsilon^p\}$ in Eqs. (14) and (15) leads to the desired relationship between increments of stress and total strain,

$$\{\Delta\sigma\} = [R]^{-1}\{\Delta\epsilon\} \tag{16}$$

where

$$[R] = [E]^{-1} + [C] \quad .$$

To obtain $\{\Delta\epsilon\}$, the linear relationship between strains and displacements may be used [15].

Relationships similar to Eq. (16) are available, relating plastic strain increments and stress increments to total strain increments for elastic-ideally plastic behavior. They are presented in Refs. 20 and 21, where the conditions that must be satisfied for ideally plastic behavior are:

- the stress increment vector must be tangential to the loading surface during continued plastic flow, and
- the strain increment vector must remain normal to the loading surface.

V. Experimental Verification

Background

After developing an analytic method to treat the nonlinear behavior of structural components, comparisons must be made with existing test data to determine the accuracy of the predictions and thereby verify that the theoretical basis of the analysis is valid. For this purpose, a few tests are usually sufficient for each major type of structure

or material behavior, but these tests should be sufficiently detailed to provide data on the distribution of strain components as well as deflections. This is because the deflections reflect the behavior of all points in the structure through a weighted integration, and the transverse motion of any local point is therefore a somewhat gross measure of the structural response. The local strains, however, are much more dependent on purely local behavior, and thus the examination of the strain distribution over the structure can provide more information on the variation of the structural behavior from point to point.

While there has been a moderate amount of test data reported to verify various elastic-plastic analysis methods [10,11, and 26 through 42], most reports show only deflections and do not report strain distributions. The notable exceptions are the tests by Ohashi and Murakami [27,28], Ohashi and Kawashima [10], and May [27] for the moderate thickness range of mild steel plates. Some earlier documents [30,31] by Ramberg, McPherson, and Levy reported strain data on very thin flat plates of large diameter-to-thickness ratios (D/h greater than 50), for which membrane behavior dominated. Of additional interest are the tests on shallow conical shells reported by Gerstle et al. [32], and the flow

patterns reported by Lance and Onat [33]. Recently, Wang and Roberts [42] have reported deformations and strains for centrally loaded spherical aluminum domes during symmetric plastic buckling.

The reports of data from cyclic tests are few. Interestingly, the early works by Ramberg et al. were on very thin aluminum plates under multiple cycles of loading in only one direction (loading and unloading with no reversals), with increasing peak loads, in which they reported residual deflections after each cycle. Haythornthwaite and Onat [11] tested a moderately thick (D/h = 40) mild steel plate, and presented central deflection versus load data for two fully reversed loading cycles with large peak deflections (up to 3 times the thickness). Ohashi and Kawashima [10] reported a test on a thick mild steel plate (D/h = 20) in which they measured the residual deflections and strains after a single cycle of loading in one direction for comparison with their theoretical prediction.

In summary, the existing test data available in the literature are inadequate for the purpose of verifying the theoretical work covering the behavior of plates of strain-hardening material in bending with large deflections, under monotonic or cyclic loads. Most of the literature is

concerned with mild steel, which allows the use of elastic-perfectly plastic analyses, except for Refs. 30 and 31, concerned with membrane behavior, and Ref. 42, concerned with buckling.

To verify the results of the present analysis, a small test program was performed on flat circular 2024-0 aluminum alloy plates with $D/h = 20.0$ and 40.6. The measured data were in the form of transverse deflections and radial and circumferential strain distributions on the upper and lower surfaces. Bending and membrane strains were calculated from the measured surface strains. These tests were specifically designed to provide the desired information to compare with the theoretical predictions, in that the material chosen had a low elastic limit stress and pronounced strain hardening behavior in the plastic range. Furthermore, a concentrated central loading was chosen because it would produce large strain gradients over the plate as compared with a distributed load, and would therefore provide a more stringent check on the analysis.

Procedure

Tests were performed on two simply supported flat plates of 2024-0 aluminum alloy, loaded by a hardened steel central

rod, as shown in Fig. 1. Both plates were 5.35 in. in diameter and had thickness of 0.1286 and 0.2615 in., while the supported diameter was 5.22 in. The loading was provided by an Instron 20,000 lb controlled deformation-rate testing machine, which also measured the load and the displacement of the loading rod. Transverse deflections were measured at points along a radial line, nominally at 0, 1, and 2 inches from the center, by three LVDT (linearly varying differential transformer) transducers. Strains were measured along another radial line at five points, nominally at 0, $\frac{1}{2}$, 1, $1\frac{5}{8}$, $2\frac{3}{8}$ in. from the center. Circumferential and radial strains were measured by strain gauges on both faces, except at the center, where only the face opposite the loading rod was instrumented. Over-all symmetry of behavior was checked by additional strain measurements at 120° intervals around the circumference at the 1-inch radius. The 21 strain gauges were of the bonded foil type (BLH Electronics, types FAET-12D-12S13ET and FAE-12S-12S13ET lot A-271) of $\frac{1}{8}$-in. sensing length using epoxy adhesive (Micro-Measurements type M-Bond GA-2) cured 1 hour at 150°F.

The tests were conducted by moving the loading rod downward against the plate at a constant nominal rate of 0.20 in./min, while the load, strains, and deflections were continuously

recorded. Since the quantity of data taken during a single test was quite large, the data reduction was performed by a time-shared digital computer with specially developed programs to transform the raw data into the desired form and providing rapid data selection for parametric studies. A cathode-ray-tube computer-graphics remote terminal, connected to the time-shared computer, was used for rapid curve plotting. Bending and membrane strains were calculated from the measured upper and lower surface strains.

Proper comparison of theory with data requires that accurate material properties data be entered into the analysis. These material properties, in the form of true stress-strain curves, were measured by means of extensive coupon tests on the same plate stock from which the circular plate specimens were cut. These coupons were taken from regions immediately adjacent to the plate specimens, and were oriented both parallel and transverse to the plate rolling axis. Extensive checkout of the strain-gauge performance was made to insure that the plastic strain data from the plates would be accurate. Each of the tension coupons had two sets of bonded strain gauges of the same type and lot as those used in the plate tests, as well as a 1-in. clip-on extensometer for comparison. The foil strain-gauges had accuracies of better than

±5 percent up to $3\frac{1}{2}$ percent strains, when checked against the clip-on extensometer. The averaged stress-strain curves for the 0.1286 and 0.2615 plate material are shown in Figs. 2a and 2b, along with faired curves for three-parameter (Ramberg-Osgood) formulas which were used in the theoretical analysis. Most data were for tension coupons, but a few tests for compression data showed stress-strain curves of nearly the same shape as for tension. The low elastic limit (about 5,000 psi stress and 0.0005 strain) of the material used was an aid in the plate tests, in that plasticity was developed at low strain levels, thereby increasing the usefulness of the strain gauges. These coupon data showed that the plate material was essentially isotropic and homogeneous.

VI. Theoretical Results and Comparison of Theoretical and Experimental Data

Plastic Analysis

To demonstrate the accuracy of the analysis for monotonic loading conditions, application of the plastic analysis alone was made to several sample structures. In addition, the behavior of these structures was investigated when they are subjected to one full cycle of loading in which the load is fully reversed. In Fig. 3 the load versus apex deflection

for a torispherical shell under uniform internal pressure is presented for various load increments, and a comparison is made with the results obtained by Khojasteh-Bakht [4]. Elastic-perfectly plastic behavior was assumed. The material properties presented in Ref. 4 were used. Khojasteh-Bakht's results were obtained by using load increments of 1.5 psi. These results are virtually identical with those of the present analysis, where a load increment of 0.4 psi was used. As seen in the figure, halving this load increment produces a significant change in the results only at a load above the theoretical collapse load predicted by limit analysis [43]. The use of the initial strain method, wherein the plastic behavior is accounted for by an "effective plastic load" vector, requires smaller load increments than a tangent modulus method [21]. However, increment size alone is not the sole criterion governing the efficiency of one method versus another. The increase in computing time associated with the use of smaller increments in the initial strain method is offset by the fact that the stiffness matrix need never be reformed after the first step. Additional evidence that indicates that the initial strain procedure is competitive from the standpoint of computer time requirements is presented in Ref. 44.

Figure 4 shows the load versus apex deflection curve for the same shell for one full cycle of loading. The load is varied between amplitudes of ±80 psi and back to zero. It is interesting to note that the deflections, moments, etc., obtained by unloading from the maximum load and subsequent loading to -80 psi are virtually the same as those that would be obtained simply by loading monotonically to -80 psi from the initial state. It is conjectured that this occurs as a combined result of assuming elastic-perfectly plastic behavior, neglecting the effects of geometric nonlinearity, and the fact that the same material properties were assumed to exist in reversed loading. Moreover, the values of residual stress, strain, and deflection obtained at the end of one full cycle are virtually the negatives of those values obtained by unloading to zero load from the maximum load.

To investigate the generality of these results, a different structure, a simply supported circular plate subjected to a uniform pressure applied centrally over a circular area with radius 0.0718 of the plate radius, was cycled through various load ranges. Again, elastic-perfectly plastic behavior was considered. The material properties assumed were $E = 10.5 \times 10^6$ psi, $\nu = 0.33$, $\sigma_o = 4000$ psi. The radius of the plate was 2.61 in. and the thickness was 0.2615 in. The

load ranges considered were ±2000, ±3000, ±3500, and ±4000 psi. The results are presented in Fig. 5. In all cases except the last, the displacements, moments, etc., at the maximum negative load obtained by unloading from the maximum positive load are the same as would be obtained merely by loading monotonically to the maximum negative load from the virgin state. For the last case (±4000 psi load range) the load increments used during reversed loading are too large from the standpoint of accuracy, and consequently the plastic strains computed are smaller than those that actually occur (4000 psi is near the theoretical collapse load of 4280 psi for this structure). These cases tend to corroborate the hypothesis that for elastic-ideally plastic materials one need only consider one-half cycle of loading to obtain information concerning full cycle behavior when the effects of geometric nonlinearity are ignored.

A strain hardening problem is considered next. A uniformly loaded clamped circular plate was cycled between ±560 psi. The same problem was considered for monotonic loading up to 560 psi by Popov et al. [45], and the results for this range are compared. Excellent agreement up to the maximum load was achieved (see Fig. 6). The discrepancies at this load may be attributed to the use of

different plasticity theories (kinematic versus isotropic hardening) and the difficulty in reproducing the stress-strain data from Ref. 45. Furthermore, the load-deflection curve does exhibit all of the characteristics of strain hardening behavior. The absolute magnitude of the center deflection at the maximum negative load is larger than that developed at the maximum positive load, and the full cycle residual deflections are triple those of the half cycle.

Results for a uniformly loaded shallow spherical shell with a stiffened circular hole at the apex are presented next. This problem demonstrates the beneficial effects of a stiffening ring on the elastic-plastic behavior of a shell, although for this particular problem it is seen that large-deflection terms are also important and should be included. The pertinent geometric and material parameters defining the problem are shown in Figs. 7 and 8. The ratio of the hole radius to shell base plane radius (b/a) is 0.1, and elastic perfectly-plastic material behavior was assumed for the shell.

Figure 7a shows the normal displacement versus the applied pressure at the ring hole interface and at an interior point approximately halfway between the hole and outer edge boundary (r = 2.5) for an unstiffened hole and one with a

stiff ring. As seen from Fig. 7a there is a substantial difference between the displacement at the hole boundary for the case of an unstiffened and for that of a stiffened hole. In fact, at the collapse load the displacement for the stiffened hole changes sign and is in the direction opposite to that of the applied uniform pressure. In effect, the region in the vicinity of the hole moves as a rigid body as the displacements in the interior become unbounded. This is due to the restraining effect of the ring in preventing the hole circumference from contracting. Since the effect of the hole is localized, the displacements in the interior (Fig. 7b) for the stiffened and unstiffened case are indistinguishable. As indicated, sudden collapse of the shell is evidenced at $qa^4/Et^4 \simeq 15000$. This occurs when the entire cross section in a substantial portion of the interior is plastic for both cases considered. However, since the ring carries a portion of the load, there is a wholly elastic section between the hole boundary and completely plastic interior cross section at collapse. This contrasts with the unstiffened case, for which the wholly plastic cross sections begin at the hole boundary and propagate towards the interior with increasing load.

Figures 8a and b show the distribution of circumferential stress resultant at the yield load and at an intermediate load in the plastic range. As expected (Fig. 8a), the peak value for the unstiffened hole is at the hole boundary. As the region of plasticity expands, this peak value moves toward the interior and is located approximately at the elastic-plastic boundary. Figure 8b shows results at the same two loads for the stiffened hole. It can be seen that the stiff ring substantially reduces the stress resultant at the hole boundary.

Geometric Nonlinearity

The accuracy of the procedure for geometric nonlinearity in the case of purely elastic behavior is considered next. Figures 9 and 10 show a comparison of results obtained from the present analysis with those obtained by Way [26] for a clamped, uniformly loaded, elastic circular plate. Poisson's ratio was chosen to be 0.3. Figure 9 is a plot of central deflection versus load, and Fig. 10 is a plot of bending and membrane stresses at the center and edge versus deflection. For the increment size chosen, excellent agreement was obtained between Way's theoretical and our numerical results.

In the present investigation, results for this problem were obtained by using both the "tangent modulus" method and

the "effective" load method for the same increment size. For the latter case, the stiffness matrix was re-formed every five increments. No equilibrium correction term was included for either method for this problem. The deflections and bending stresses in both cases were identical, while slightly smaller membrane stresses were predicted by the effective load method. Of most significance was the reduction in CPU time from 386.28 seconds for the tangent modulus method to 202.08 seconds for the effective load method, and approximately 47 percent time savings at no appreciable loss in accuracy. Similar time savings of from 40 to 50 percent were noted for other problems.

Figure 11 illustrates the need for the equilibrium correction term in problems involving a high degree of nonlinearity. An exact load-deflection curve obtained from Ref. 22, based upon results presented in Ref. 46, is shown for an elastic, clamped spherical cap loaded by a central concentrated load. Also shown are results obtained from the current analysis using a straight incremental approach with 1/8 lb increments and an incremental-plus-equilibrium correction solution using 1 lb increments. The results obtained in the current analysis are virtually identical (for

both incremental and incremental-with-equilibrium correction solutions) to the numerical results given in Ref. 22.

Combined Material and Geometric Nonlinearity

Figure 12 shows a load versus central deflection plot for a centrally loaded, simply-supported plate with a diameter-to-thickness ratio of 40.6. The numerical results are compared with test data obtained from the experimental program described in Section V. Shown are the linear elastic, nonlinear elastic, elastic-plastic and combined nonlinear predictions using the tangent modulus approach with the incremental and incremental-with-equilibrium correction solution procedures. Although for these combined problems the equilibrium correction affords a considerable improvement over the incremental approach, without equilibrium correction, a more extensive iteration scheme is probably needed to close the theoretical-experimental gap. In Figs. 13 and 14 the radial distribution of circumferential strain at the lower and upper surfaces, respectively, for this plate is illustrated for several load levels and compared with theory. Despite the only fair-to-good correlation of the displacement data at high loads, excellent correlation with experiment for the strains is noted, except,

as might be anticipated, directly under the loading rod for higher loads. The discrepancy at this point might be the result of local shear and penetration effects.

The next two figures, Figs. 15 and 16, present load-deflection and strain data for a thicker plate with a diameter-to-thickness ratio of 20.0. Figure 15 is a plot of the deflections at the center and one inch from the center versus load, and Fig. 16 presents the circumferential strain distributions at the upper and lower surfaces. Again, the equilibrium correction leads to much more accurate predictions, and at high loads there is better strain correlation than deflection correlation.

Wilkinson and Fulton [47] have presented results for the elasto-plastic buckling of uniformly loaded shallow spherical caps with both simple and clamped support at the edges. Several comparison test cases were chosen to verify their results and determine the present program's ability to predict buckling loads of such structures. The cases run were for $\alpha = 0.1$, $\beta = 0.002$, and $\lambda = 4$ and 5.5 for the clamped cap, and $\lambda = 4$ for the simply supported cap. Here α is the ratio of tangent modulus to Young's modulus, β is the ratio of yield stress to Young's modulus, and λ is the geometric shell parameter $2[3(1 - \nu^2)]^{\frac{1}{4}}(H/h)^{\frac{1}{2}}$, with

ν being Poisson's ratio, H the maximum shell rise, and h the shell thickness. As can be seen from Fig. 17, excellent agreement for these cases was obtained. The buckling pressures were about 3 percent higher than those predicted by Wilkinson and Fulton. Their results are probably more accurate, since the present analysis makes no attempt to refine the load increment size in the vicinity of the critical load. The tangent modulus method was used for the large-deflection effects.

Results in the form of load versus central deflection of a simply supported, centrally loaded mild steel circular plate are shown in Fig. 18. These results involve a history of loading to a maximum load in the plastic range and then the removal of the load. A comparison with the experimental data presented in Ref. 11 indicates that the finite-element results predict larger displacements than those obtained experimentally. This may be partially explained by the fact that no information (except the yield stress) was available in Ref. 11 concerning the strain hardening properties of the material used in the experiment. The finite-element analysis was performed by assuming elastic-ideally plastic behavior, which is a good representation of the stress-strain behavior

for mild steel as long as the strains are smaller than about 2 percent. The larger displacement prediction from analysis is consistent with this assumption. When the strains in the plate become larger than 2 percent, mild steel experiences strain hardening. Indeed at loads above 15,000 lb the theoretically predicted strains exceed 2 percent in a considerable region of the plate, and divergence of the results occurs. As a consequence of the overprediction of the maximum displacement, the residual displacement predicted by the analysis is considerably greater than that experimentally observed. However, the general shape of the load-deflection curve upon unloading parallels the experimental curve.

In the next figure, Fig. 19, a simply-supported, centrally-loaded circular plate with the same dimensions and material properties as the plate used in the experimental program was loaded through a half cycle to evaluate the strain hardening cyclic loading feature of the program. Geometric nonlinearity was included. The load was increased from zero to 1600 psi, which is well into the plastic range for this specimen, and back to zero to obtain residual stresses, strains, and displacements.

No strain hardening experimental data are yet available for the unloading portion of the load regime. However, the

1600 psi maximum load (177 lb total load) is not sufficiently large to introduce appreciable geometric nonlinearities (see Fig. 12). The results have been compared with our small strain, small-deflection, elasto-plastic results, and the correlation is seen to be excellent. This correlation verified that the procedural aspects of the large-deflection cyclic analysis are correct.

VI. Conclusions

A large-deflection elastic-plastic analysis using an incremental finite-element approach has been developed to predict the behavior of shells of revolution under cyclic loading conditions. Good agreement with both theoretical and experimental predictions has been obtained for problems involving monotonic loading. In the case of cyclic loading with load reversal, limited test data are available for the unloading and reversed loading segments of the load cycle. The qualitative agreement in these regions is good, and a more detailed quantitative evaluation will be made when the anticipated test data from a planned series of experiments become available. It is also desirable to incorporate into the analysis the capability for traversing unstable portions of the load-deflection curve (e.g., through displacement

control). This capability is important for predicting post-buckling behavior and plastically-induced instabilities encountered during reversed loading situations [11]. Various methods for large-deflection elastic and elasto-plastic problems have been proposed [48,49]. Adaptation and evaluation of these methods for the combined nonlinear problem is a desirable, and has recently become an attainable, goal.

Appendix

Shell Element

The geometry of the element is presented in Fig. 20. The approach employed is basically an extension of the work presented by Khojasteh-Bakht [4] to include cubic polynomials in the representation of the meridional displacement. It differs from other similar formulations [50,51] in that Hermitian instead of Lagrangian interpolation is used for the meridional displacement. The additional degree of freedom required at each node, the linear meridional membrane strain, ϵ_s^L, ensures compatibility of all membrane strains. In Refs. 50 and 51, where Lagrangian interpolation is employed for the meridional displacement, the "intermediate" displacements are statically condensed out, reducing the over-all size of the stiffness matrix. This leads to smaller solution times at the expense of accuracy in the membrane strain predictions.

In the element derivation, Sanders' nonlinear shell theory [52] (modified to include orthotropic shell properties) for small strains and moderate rotations is used as the basis of the analysis. Thus we have for the strain-displacement relations,

$$\begin{Bmatrix} \epsilon_s \\ \\ \epsilon_\theta \end{Bmatrix} = \begin{Bmatrix} \epsilon_s^o \\ \\ \epsilon_\theta^o \end{Bmatrix} + \zeta \begin{Bmatrix} \kappa_s \\ \\ \kappa_\theta \end{Bmatrix} \tag{A-1}$$

where ζ is the distance from the shell middle surface in the direction normal to the shell. Here ϵ_s, ϵ_θ are the total strains in the meridional and circumferential directions, respectively. Furthermore,

$$\epsilon_s^o = \frac{du}{ds} + \frac{w}{R_1} + \tfrac{1}{2}\chi^2$$
$$\epsilon_\theta^o = \frac{1}{r}(u \cos \varphi + w \sin \varphi) \tag{A-2}$$

are the middle surface strains, and the curvatures are given by

$$\kappa_s = -\frac{d\chi}{ds}$$
$$\kappa_\theta = -\frac{\cos \varphi}{r}\chi \ . \tag{A-3}$$

The meridional rotation χ is

$$\chi = \frac{dw}{ds} - \frac{u}{R_1} \ . \tag{A-4}$$

The stress-strain relations for an orthotropic axisymmetric body with principal axes in the meridional and circumferential directions are:

$$\begin{Bmatrix} \sigma_s \\ \sigma_\theta \end{Bmatrix} = \begin{bmatrix} C_{ss} & C_{s\theta} \\ C_{\theta s} & C_{\theta\theta} \end{bmatrix} \begin{Bmatrix} \epsilon_s^e \\ \epsilon_\theta^e \end{Bmatrix} \tag{A-5}$$

$$= [E]\{\epsilon^e\} \quad .$$

The vector $\{\epsilon^e\}$ is the vector of elastic strains. In terms of Young's modulus E and Poisson's ratio ν, the elements of the material properties matrix $[E]$ are:

$$C_{ss} = \frac{E_s}{1 - \nu_{\theta s}\nu_{s\theta}} \quad ; \quad C_{s\theta} = \frac{E_s \nu_{s\theta}}{1 - \nu_{\theta s}\nu_{s\theta}}$$

$$C_{\theta s} = \frac{E_\theta \nu_{\theta s}}{1 - \nu_{\theta s}\nu_{s\theta}} \quad ; \quad C_{\theta\theta} = \frac{E_\theta}{1 - \nu_{\theta s}\nu_{s\theta}} \quad . \tag{A-6}$$

From energy considerations, $C_{s\theta} = C_{\theta s}$. We may represent the local Cartesian shell displacements u_1, u_2 as

$$u_\alpha = \sum_{i=1}^{2} H_{oi}^{(1)}(\xi) u_{\alpha_i} + H_{1i}^{(1)}(\xi) u_{\alpha,\xi i} \quad \alpha = 1,2$$

or (A-7)

$$\{u\} = [\bar{N}]\{u_c\}$$

where $H_{oi}^{(1)}(\xi)$ and $H_{1i}^{(1)}(\xi)$ are cubic Hermitian interpolation polynomials, and $\{u_c\}$ is the vector of Cartesian generalized displacements.

The strain-displacement relations may now be written in terms of the rectilinear displacements u_1, u_2 with the independent variable changed from arc length s to normalized chord variable ξ (see Fig. 20). The differential relationship between s and ξ is

$$ds = \frac{\ell \, d\xi}{\cos \beta} \tag{A-8}$$

where ℓ is the element chord length, β is the angle between the tangent to the substitute curve $\eta = \eta(\xi)$ and the ξ axis, i.e.,

$$\frac{d\eta}{d\xi} = \tan \beta \quad . \tag{A-9}$$

We obtain the following matrix relations for the linear strains

$$\begin{aligned} \{e\} = \{\epsilon_L^o\} + \zeta\{\kappa\} &= \left[[\bar{W}_m] + \zeta[\bar{W}_b]\right]\{u_c\} \\ &= [\bar{W}]\{u_c\} \quad . \end{aligned} \tag{A-10}$$

Here $\{e\}$ is the vector of linear strains and $\{\epsilon_L^o\}$ is the linear contribution to the membrane strains.

The Cartesian displacements and their derivations with respect to the normalized chord variable ξ (see Fig. 20) may be related to the tangential and normal displacements, the rotation χ, and the linear meridional membrane strain through the transformation,

$$\begin{Bmatrix} u_1 \\ u_2 \\ u_{1,\xi} \\ u_{2,\xi} \end{Bmatrix} = \begin{bmatrix} \cos\beta & -\sin\beta & 0 & 0 \\ \sin\beta & \cos\beta & 0 & 0 \\ 0 & 0 & -\ell\tan\beta & \ell \\ 0 & 0 & \ell & \ell\tan\beta \end{bmatrix} \begin{Bmatrix} u \\ w \\ \chi \\ \epsilon_s^L \end{Bmatrix}$$

or (A-11)

$$\{u_c\} = [T]\{u_s\} \quad .$$

Using these relationships in Eq. (A-10) and Eq. (A-7), respectively, we obtain

$$\{e\} = [\bar{W}]\{u_c\} = [\bar{W}][T]\{u_s\} = [W]\{u_s\} \qquad \text{(A-12)}$$

and

$$\{u\} = [\bar{N}][T]\{u_s\} = [N]\{u_s\} \quad . \qquad \text{(A-13)}$$

The geometry of the curved element, $\eta = \eta(\xi)$, may be represented by various interpolation polynomials as well. Cubic and fifth order Hermitian interpolation or third order Lagrangian interpolation is available in the program. From Eqs. (A-5) and (A-12), the final form of the element stiffness matrix is [see Eq. (11)]:

$$[k^{(0)}] = \int_V [W]^T[E][W]dV \quad .$$

Details of the formulation of the element stiffness matrix, including the elements of the [W] and [N] matrices, are presented in Ref. 14, along with a group of sample problems illustrating the accuracy of the elements for linear elastic problems.

The consistent load vector for the applied surface tractions is obtained from Eq. (11). The applied pressures are allowed to vary linearly from node to node, i.e.,

$$\{\Delta T^{(0)}\} = \{\Delta T_i^{(0)}\}(1 - \xi) + \{\Delta T_j^{(0)}\}\xi \quad . \tag{A-14}$$

We then have for the consistent load vector

$$\{\Delta P_i\} = \int_A [N]^T \{\Delta T^{(0)}\} dA \quad . \tag{A-15}$$

For the small-strain, moderate-rotation problems considered here, i.e., for the strain-displacement relations presented in Eqs. (A-1) through (A-4), the initial-stress stiffness matrix may be written as

$$[k^{(1)}] = \int_V S_s [\Omega]^T [\Omega] dV \tag{A-16}$$

where $[\Omega]$ is the matrix relating the rotations χ to the nodal degrees of freedom, i.e.,

$$\{\chi\} = [\Omega]\{u_s\} \quad . \tag{A-17}$$

Normally, S_s is assumed to be constant throughout the element and is evaluated at the centroid of the element. In the present analysis, S_s was assumed to vary linearly from node to node so that nodal values could be used, since stress computations were carried out at these locations. This leads to:

$$[k^{(1)}] = \int_A \int_{-h/2}^{h/2} \left[S_s^i(1 - \xi) + S_s^j\xi\right][\Omega]^T[\Omega]d\zeta \, dA$$

or (A-18)

$$[k^{(1)}] = N_{s_i} \int_A [\Omega]^T[\Omega](1 - \xi)dA + N_{s_j} \int_A [\Omega]^T[\Omega]\xi dA \quad .$$

where h is the shell thickness.

We must now evaluate the initial-strain matrix (effective plastic load vector), given by Eq. (11) to be

$$\{\Delta Q_i\} = \int_V [W]^T[E]\{\Delta\epsilon^P\}dV \quad . \tag{A-19}$$

We assume that the incremental initial (plastic) strains vary linearly from node to node, while at the nodes the variation of the plastic strains through the thickness is arbitrary. This may be expressed as:

$$\{\Delta\epsilon^P(\xi,\zeta)\} = \{\Delta\epsilon^P(0,\zeta)\}(1 - \xi) + \{\Delta\epsilon^P(1,\zeta)\}\xi \quad . \quad \text{(A-20)}$$

Substituting Eq. (A-20) into Eq. (A-19), we get

$$\{\Delta Q_i\} = \int_A \int_{-h/2}^{h/2} [W]^T[E]\Big[\{\Delta\epsilon^P(0,\zeta)\}(1 - \xi) + \{\Delta\epsilon^P(1,\zeta)\}\xi\Big]d\zeta \, dA$$

or since

$$[W] = [W_m] + \zeta[W_b]$$

$$\begin{aligned}\{\Delta Q_i\} = &\int_A (1 - \xi)[W_m]^T[E]dA \left[\int_{-h/2}^{h/2} \{\Delta\epsilon^P(0,\zeta)\}d\zeta\right] \\ &+ \int_A \xi[W_m]^T[E]dA \left[\int_{-h/2}^{h/2} \{\Delta\epsilon^P(1,\zeta)\}d\zeta\right] \\ &+ \int_A (1 - \xi)[W_b]^T[E]dA \left[\int_{-h/2}^{h/2} \zeta\{\Delta\epsilon^P(0,\zeta)\}d\zeta\right] \\ &+ \int_A \xi[W_b]^T[E]dA \left[\int_{-h/2}^{h/2} \zeta\{\Delta\epsilon^P(1,\zeta)\}d\zeta\right] \quad .\end{aligned} \quad \text{(A-21)}$$

The evaluation of the "effective plastic" moments and forces through the thickness was carried out by using Simpson's rule

with 11 or 21 integration points. All area integrations (actually integrations with respect to ξ) were performed by using a Gauss-Legendre integration scheme of sixth order. Although a sixth order scheme was probably excessive, a convergence study for the stiffness properties showed it always gave good results.

Thin Ring Stiffener Element

For many structural designs, local stiffeners are needed for added strength in regions of high stress intensity. To be able to analyze the effects such stiffeners have on the development of plastic regions, a ring stiffener element was included in the analysis. The ring used is identical to the one proposed by Cohen [53] (except for the fact that it may be attached with arbitrary eccentricity).

References

1. D. Bushnell, "Nonlinear Axisymmetric Behavior of Shells of Revolution," AIAA J., 5, 3, 432-439 (1967).
2. A. Kalnins and J. F. Lestingi, "On Nonlinear Analysis of Elastic Shells of Revolution," J. Appl. Mech., 34, 1, 59-67,(1967).
3. J. A. Stricklin, N. E. Haisler, H. R. MacDougall, and F. J. Stebbins, "Nonlinear Analysis of Shells of Revolution by the Matrix Displacement Method," AIAA J., 6, 12, 2306 (1968).
4. M. Khojasteh-Bakht, "Analysis of Elastic-Plastic Shells of Revolution under Axisymmetric Loading by the Finite Element Method," Ph.D. dissertation, University of California at Berkeley, SESM67-8 (1967).
5. P. V. Marcal and C. E. Turner, "Elastic-Plastic Behavior of Axisymmetrically Loaded Shells of Revolution," J. Mech. Eng. Sci., 5, 3, 232 (1963).
6. E. A. Witmer and J. J. Kotanchik, "Progress Report on Discrete-Element Elastic and Elastic-Plastic Analyses of Shells of Revolution Subjected to Axisymmetric and Asymmetric Loading," Pro. Air Force 2nd Conf. on Matrix Methods in Structural Mechanics, Wright-Patterson AFB, Ohio, AFFDL-TR-68-150 (1968).

7. P. V. Marcal, "Large Deflection Analysis of Elastic-Plastic Shells of Revolution," AIAA J., 8, 9, 1627 (1970).

8. L. A. Hofmeister, G. A. Greenbaum, and D. A. Evensen, "Large Strain, Elasto-Plastic Finite Element Analysis," AIAA J., 9, 7, 1248 (1971).

9. S. Yaghmai, Incremental Analysis of Large Deformations in Mechanics of Solids with Applications to Axisymmetric Shells of Revolution, NASA CR-1350 (1969).

10. Y. Ohashi and K. Kawashima, "On the Residual Deformation of Elasto-Plastically Bent Thin Circular Plates After Perfect Unloading," Z.A.M.M., 49, 5, 275-286 (1969).

11. R. M. Haythornthwaite and E. T. Onat, "The Load Carrying Capacity of Initially Flat Circular Steel Plates under Reversed Loading," J. Aero. Sci., 22, 12, 867 (1955).

12. W. Prager, "A New Method of Analyzing Stress and Strains in Work-Hardening Plastic Solids," J. Appl. Mech., 23, 493 (1956).

13. H. Ziegler, "A Modification of Prager's Hardening Rule," Quart. Appl. Math., 17, 1, 55 (1959).

14. H. S. Levine and H. Armen, Jr., A Refined Doubly-Curved Axisymmetric Orthotropic Shell Element, Grumman Res. Dept. Memorandum RM-496 (1971).

15. M. A. Biot, Mechanics of Incremental Deformations, John Wiley & Sons, Inc., New York (1965).

16. T. H. Lin, Theory of Inelastic Structures, John Wiley & Sons, Inc., New York (1968).

17. R. H. Gallagher, J. Padlog, and P. P. Bijlaard, "Stress Analysis of Heated Complex Shapes," J. Am. Rocket Soc., 32, 700-707 (1962).

18. C. A. Felippa, "Refined Finite Element Analysis of Linear and Nonlinear Two Dimensional Structures," Structures and Materials Research Report, Department of Civil Engineering Report No. 66-22, Univ. of California, Berkeley (1966).

19. R. H. Mallett and P. V. Marcal, "Finite Element Analysis of Nonlinear Structures, Proc. of the A.S.C.E., J. of the Structures Division, 94, ST9,(1968).

20. G. Isakson, H. Armen, Jr., and Pifko, A., "Discrete-Element Methods for the Plastic Analysis of Structures," NASA CR-803 (1967).

21. H. Armen, Jr., A. B. Pifko, and H. S. Levine, Finite Element Analysis of Structures in the Plastic Range, Grumman Res. Dept. Report RE-381 (1970); also NASA CR-1649 (1971).

22. W. Haisler and J. Stricklin, "Development and Evaluation of Solution Procedures for Geometrically Nonlinear Structural Analysis by the Direct Stiffness Method," presented at AIAA/ASME 12th Structures, Structural Dynamics and Materials Conference, Anaheim, California (1971).

23. R. Hill, The Mathematical Theory of Plasticity, Chapter 12, Oxford University Press (1950).

24. D. C. Drucker, "A More Fundamental Approach to Plastic Stress-Strain Relations," Proc. First U.S. National Congress of Applied Mechanics (Chicago, 1951), 487, New York (1952).

25. W. Ramberg and W. R. Osgood, "Description of Stress-Strain Curves by Three Parameters," NACA TN 902 (1943).

26. S. Way, "Bending of Circular Plates with Large Deflection," Trans. ASME, 56, 627-636 (1934).

27. Y. Ohashi and S. Murakami, "Large Deflection in Elasto-plastic Bending of a Simply Supported Circular Plate Under a Uniform Load," J. Appl. Mech., Trans. ASME, 866-870 (1966).

28. Y. Ohashi and S. Murakami, "The Elasto-Plastic Bending of a Clamped Thin Circular Plate," Proc. 11th Int. Cong. Applied Mechanics, Munich, 212-223 (1964).

29. G. May, "Elastic Plastic Behavior of Plates," U. of Colorado, Ph.D. Thesis, University Microfilms, Ann Arbor, Michigan (1967).

30. W. Ramberg, A. McPherson, and S. Levy, "Normal-Pressure Tests of Rectangular Plates," NACA Tech. Note 849 (1942).

31. A. McPherson, W. Ramberg, and S. Levy, "Normal Pressure Tests of Circular Plates with Clamped Edges," NACA Report 744 (1942).

32. K. Gerstle, R. Lance, and E. Onat, "Plastic Behavior of Conical Shells," Proc. 1st Southeastern Conf. Theoretical and Applied Mechanics (1962). Developments in Theoretical and Applied Mechanics, 1, Plenum Press, New York (1963).

33. R. Lance and E. Onat, "Comparison of Experiments and Theory in the Plastic Bending of Circular Plates," J. Mech. Phys. Solids, Pergammon Press, 10, 301-311 (1962).

34. P. Naghdi, "Bending of Elastoplastic Circular Plates with Large Deflection," J. Appl. Mech., ASME, 293-300 (1952).

35. R. Haythornthwaite, "Deflection of Plates in the Elastic-Plastic Range," Second U.S. Nat. Congr. Appl. Mech., 521-526 (1954).

36. R. Cooper and G. Shifrin, "Experiment on Circular Plates in the Plastic Range," Second U.S. Nat. Congr. Appl. Mech., 527-534 (1954).

37. W. Olszak and A. Sawczuk, "Experimental Verification of Limit Analysis of Plates, Part I," Bull. l'Acad. Polonaise des Sciences, Cl. IV, III, 4, 195-200 (in English) (1955).

38. J. Foulkes and E. Onat, "Tests of Behavior of Circular Plates Under Transverse Load," Brown U., Div. of Engineering Report OOR 3172/3 (1955).

39. E. Onat and R. Haythornthwaite, "Load Carrying Capacity of Circular Plates at Large Deflection," J. Appl. Mech., ASME, 23, 49-55 (1956).

40. S. Lerner and W. Prager, "On the Flexure of Plastic Plates," J. Appl. Mech., ASME, 353-354 (1960).

41. N. Srivastava and A. Sherbourne, "Elastic Plastic Bending of Circular Plates," J. Engineering Mechs. Div. ASCE, 13-31 (1971).

42. S. Wang and S. Roberts, "Plastic Buckling of Point-Loaded Spherical Shells," J. Engineering Mechs. Div. ASCE, 77-93 (1971).

43. D. C. Drucker and R. T. Shield, "Limit Analysis of Symmetrically Loaded Thin Shells of Revolution," J. Appl. Mech., 26, 1, 61-68 (1959).

44. K. S. Havner, "On Convergence of Iterative Methods in Plastic Strain Analysis," Int. J. Solids and Structures, 4, 491-508 (1968).

45. E. Popov, M. Khojasteh-Bakht, and S. Yaghmai, "Bending of Circular Plates of Hardening Material," Int. J. Solids and Structures, 3, 975-988 (1967).

46. J. F. Mescall, "Large Deflections of Spherical Shells Under Concentrated Loads," J. of Appl. Mech., 32, 4, 936-938 (1965).

47. M. Wilkinson and R. Fulton, "Axisymmetric Buckling of Uniformly Loaded Spherical Caps Undergoing Plastic Deformation," in preparation (1972).

48. P. Sharifi and E. P. Popov, "Nonlinear Buckling Analysis of Sandwich Arches," J. of the Eng. Mech. Div., Proc. of the A.S.C.E., 97, EM5 (1971).

49. O. C. Zienkiewicz, "Incremental Displacement in Non-Linear Analysis," Int. J. for Numerical Methods in Eng., 3, 4, 587-592 (1971).

50. P. M. Mebane and J. A. Stricklin, "Implicit Rigid Body Motion in Curved Finite Elements," AIAA J., 9, 2, 344-345 (1971).

51. E. P. Popov and P. Sharifi, "A Refined Curved Element for Thin Shells of Revolution," Int. J. for Numerical Methods in Eng., 3, 4, 495-508 (1971).

52. J. L. Sanders, Jr., "Nonlinear Theories for Thin Shells," Quarterly Appl. Math., 21, 1, 21-36 (1963).

53. G. Cohen, "Computer Analysis of Asymmetric Buckling of Ring-Stiffened Orthotropic Shells of Revolution," AIAA J., 6, 1 (1968).

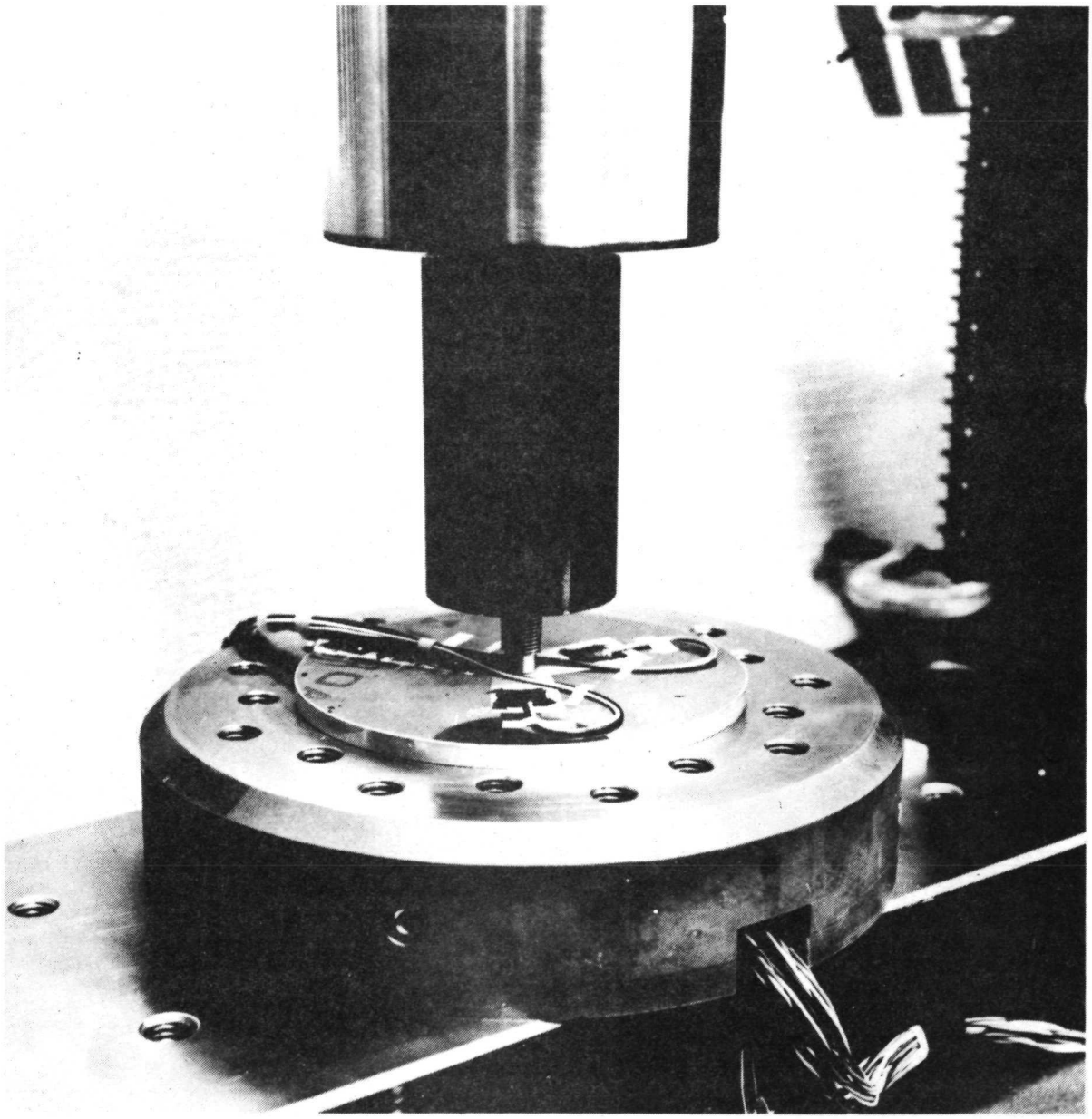

Fig. 1 A Plate Specimen in Fixture

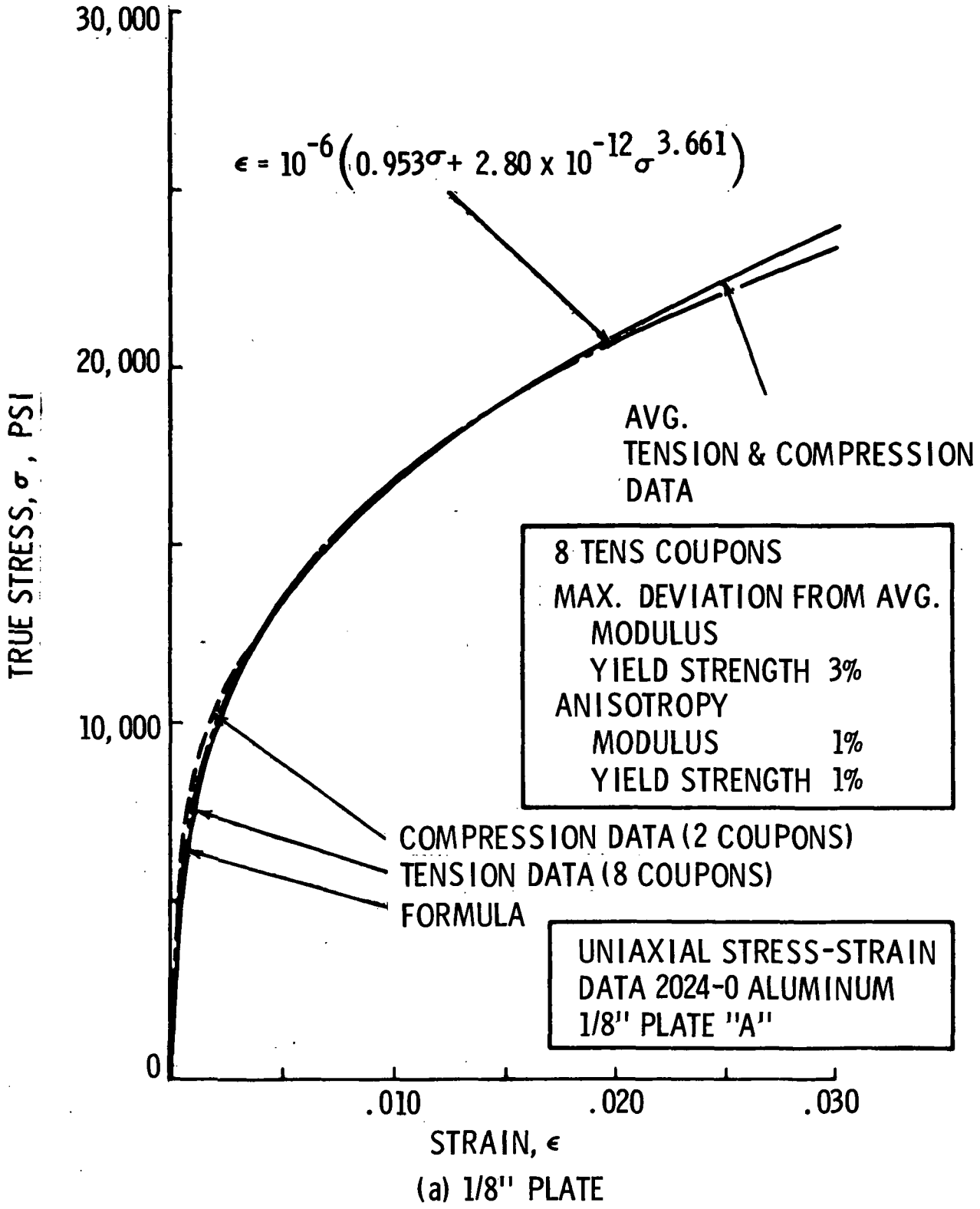

(a) 1/8" PLATE

FIG. 2 UNIAXIAL STRESS-STRAIN DATA FOR 2024-0 ALUMINUM PLATES

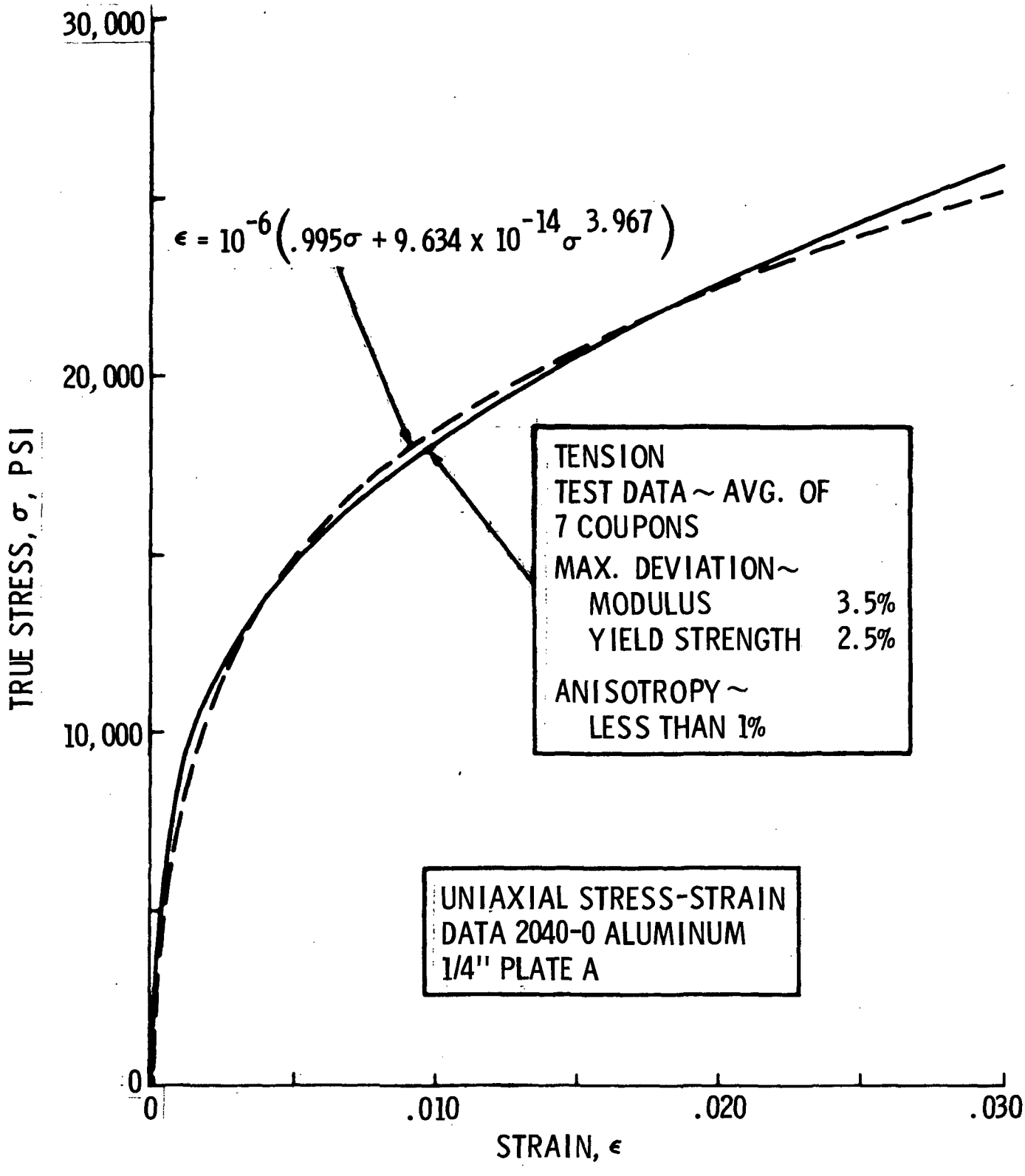

(b) 1/4" PLATE

FIG. 2 UNIAXIAL STRESS-STRAIN DATA FOR 2024-0 ALUMINUM PLATES

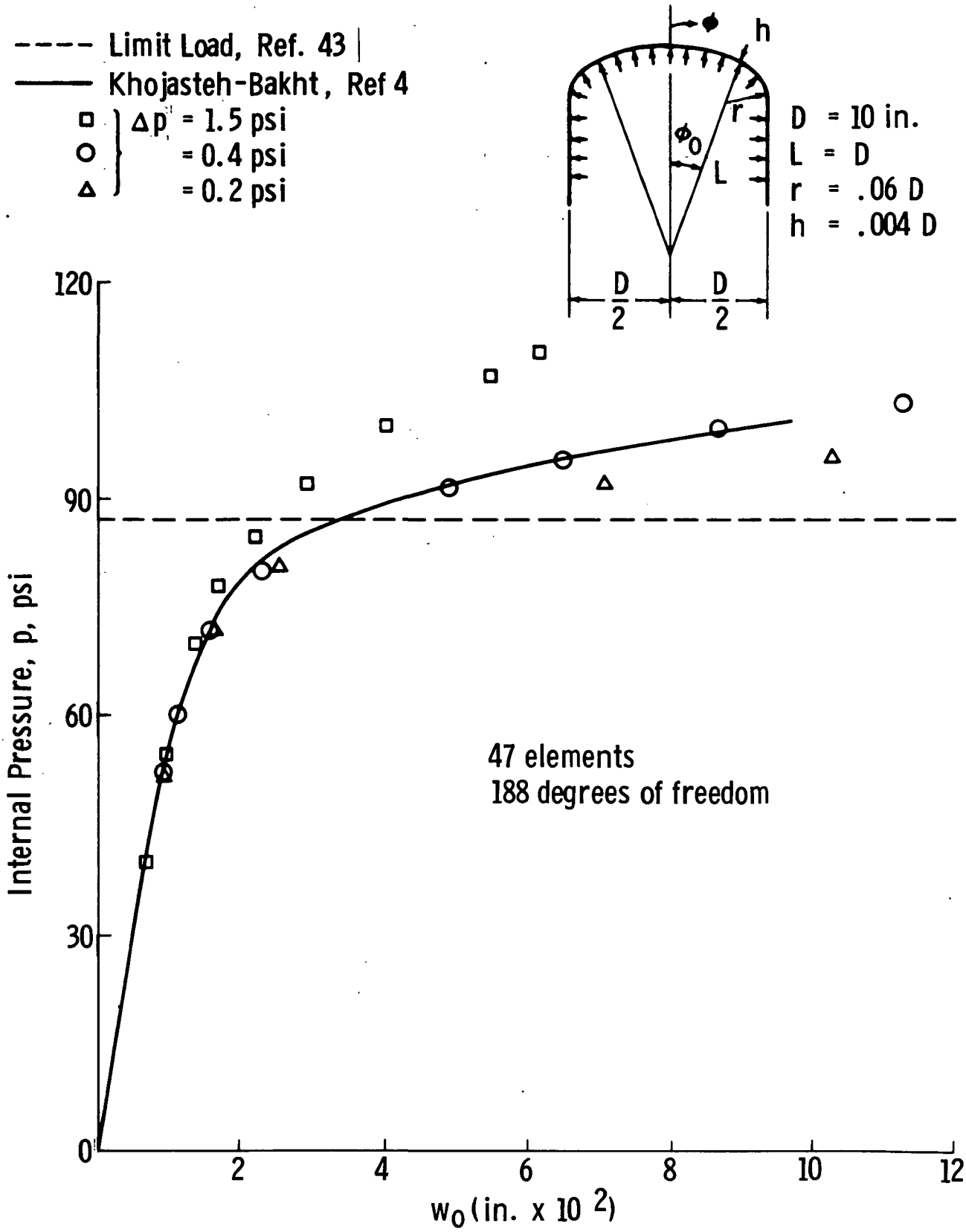

FIG. 3 PRESSURE VERSUS NORMAL DISPLACEMENT, w_0, AT APEX ($\phi = 0°$) FOR DIFFERENT LOAD INCREMENTS - TORISPHERICAL SHELL

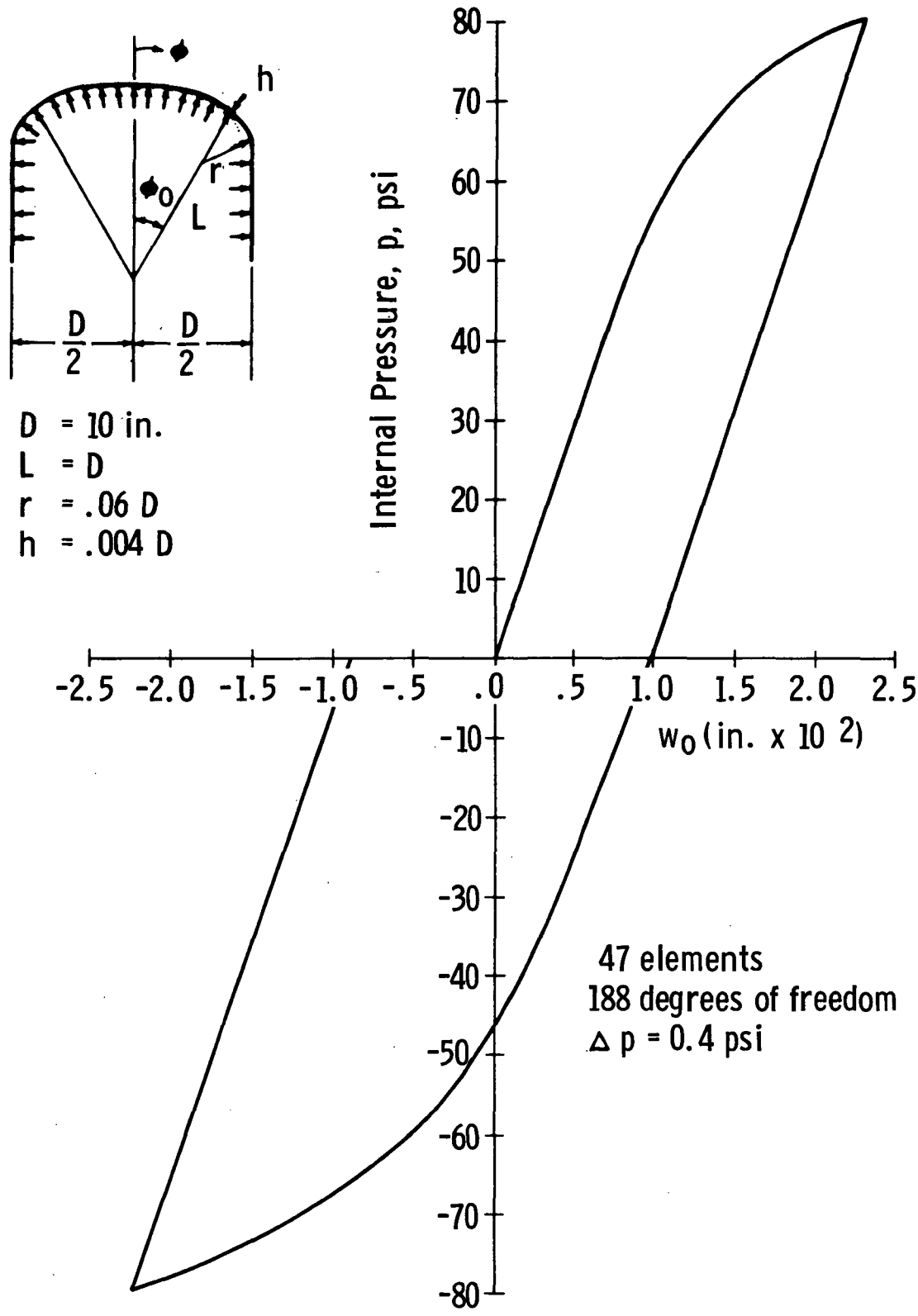

FIG. 4 CYCLIC PRESSURE VERSUS NORMAL DISPLACEMENT, w_o, AT APEX ($\phi = 0°$) TORISPHERICAL SHELL

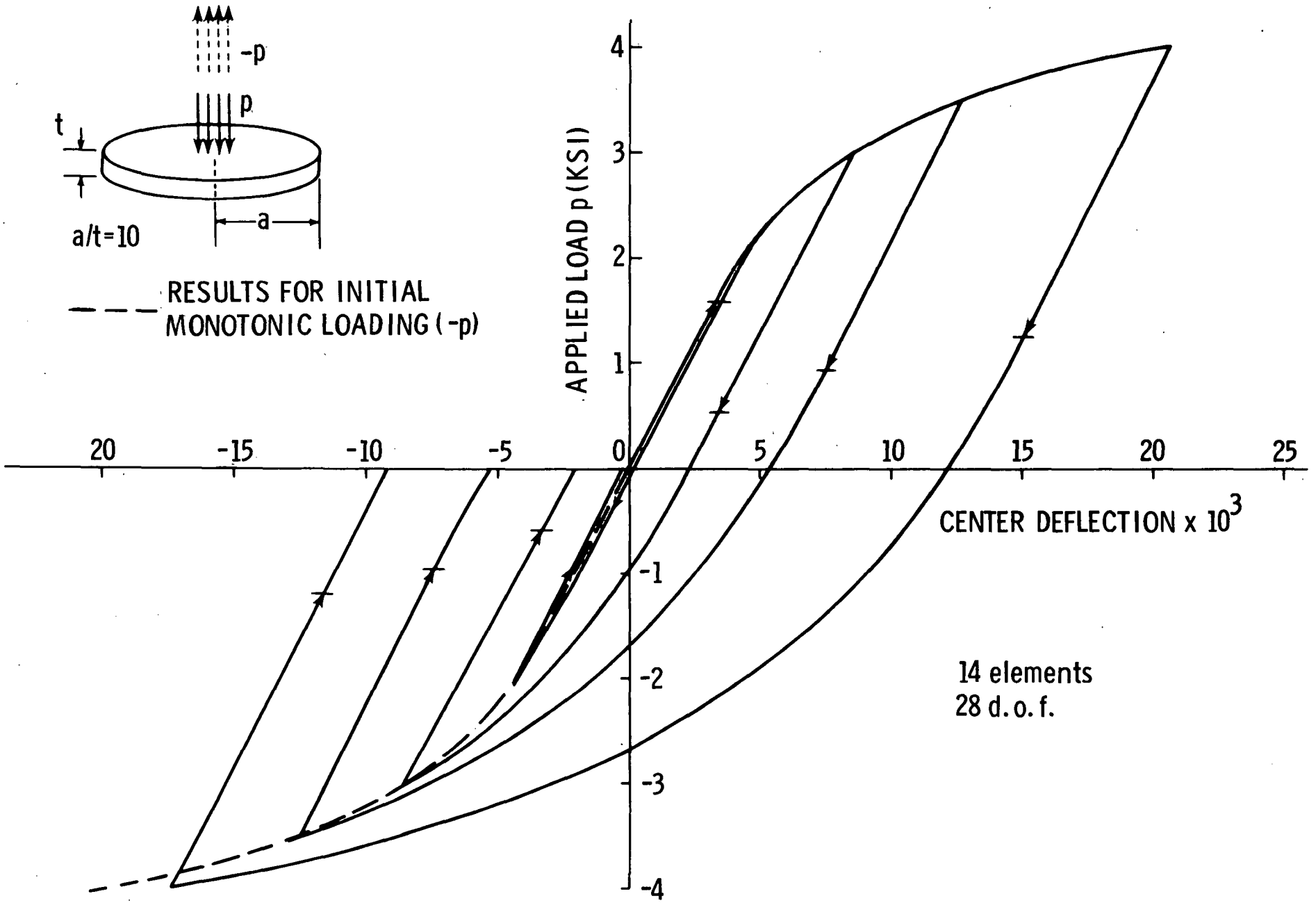

FIG. 5 LOAD VERSUS CENTER DEFLECTION OF A SIMPLY SUPPORTED, CENTRALLY LOADED CIRCULAR PLATE

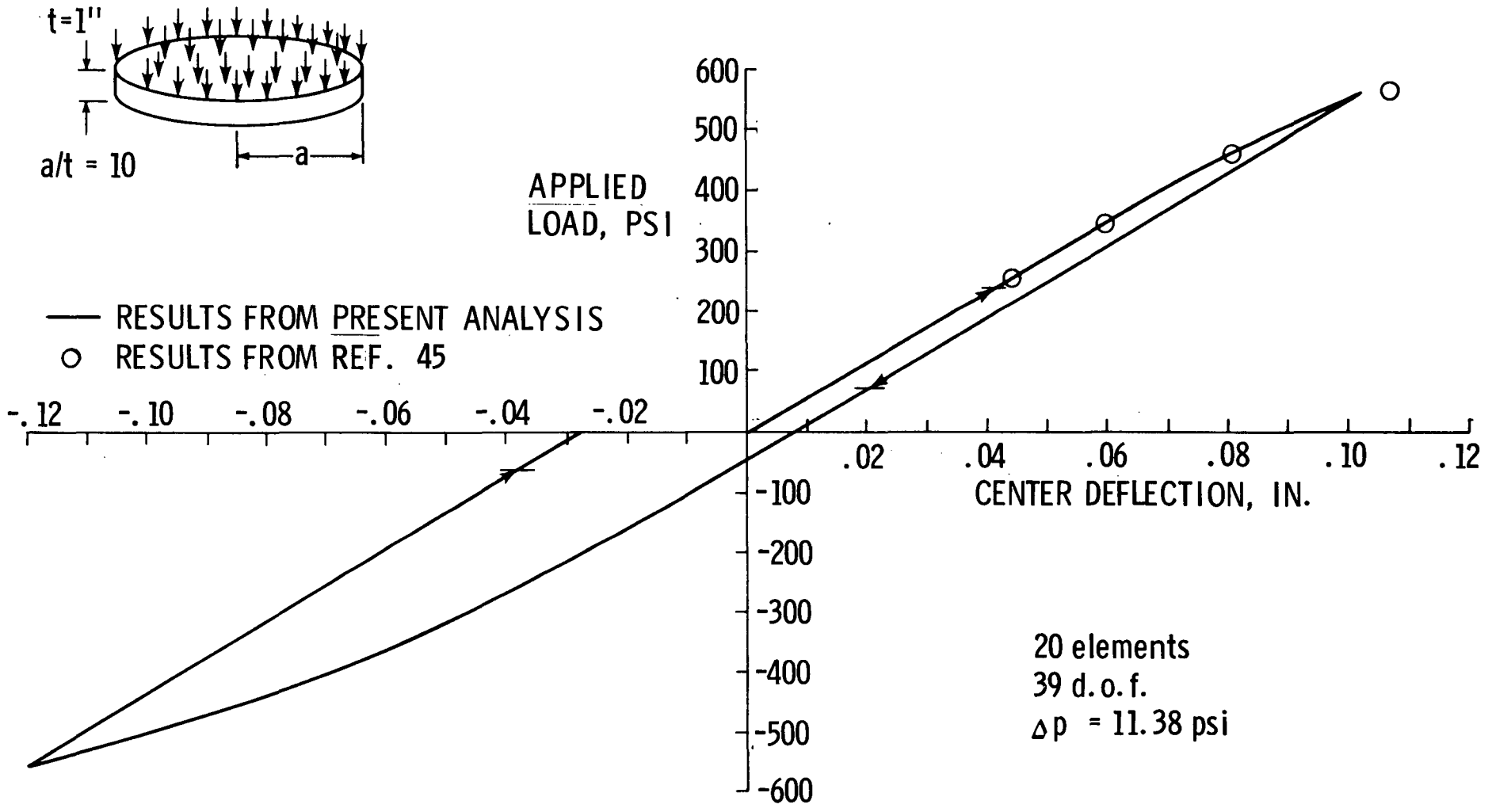

FIG. 6 LOAD VERSUS CENTER DEFLECTION OF A UNIFORMLY LOADED CLAMPED CIRCULAR PLATE

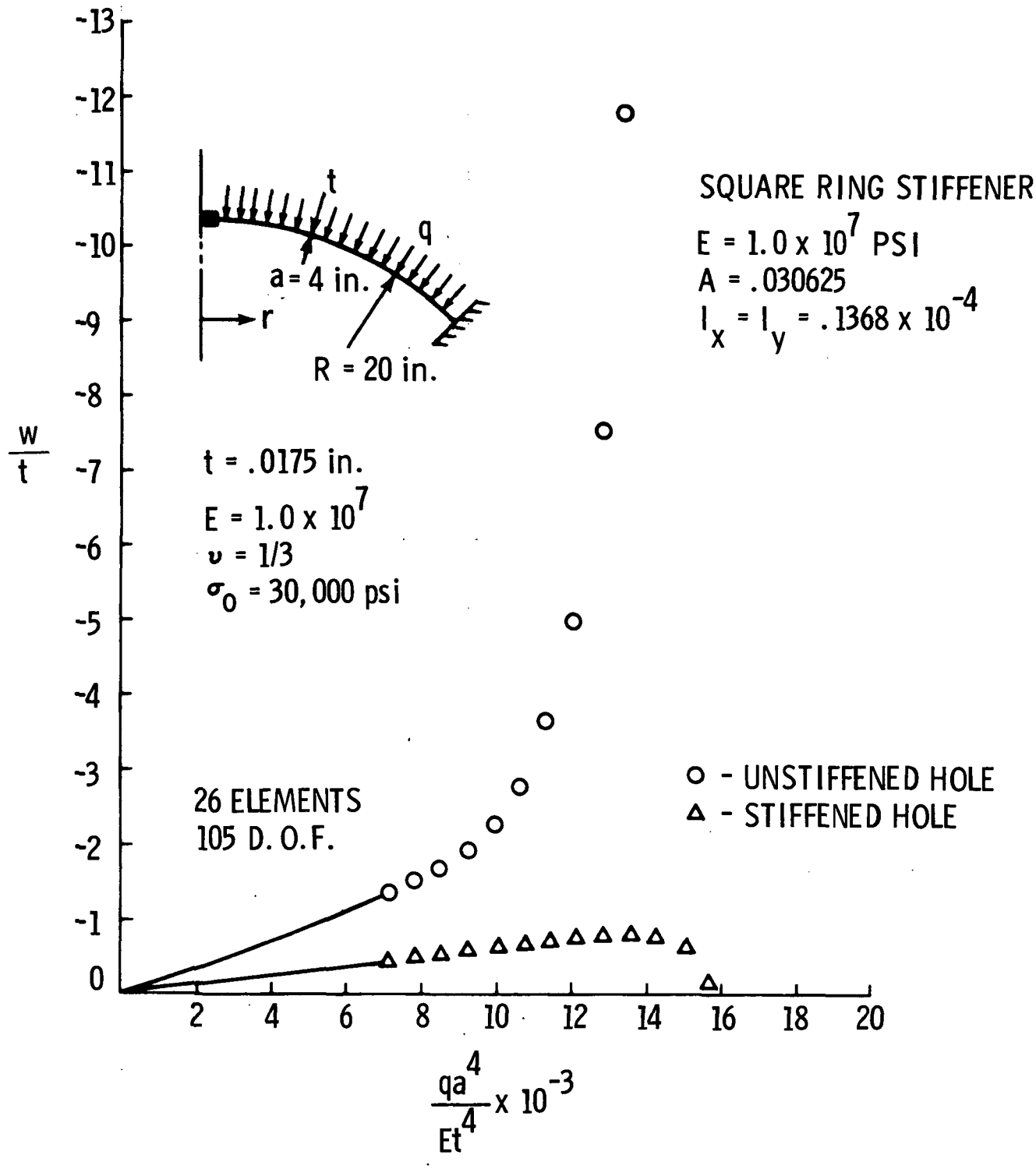

(a) NORMAL DISPLACEMENT AT THE HOLE BOUNDARY

FIG. 7 LOAD-DEFLECTION CURVES FOR RING-STIFFENED SPHERICAL SHELL UNDER EXTERNAL PRESSURE

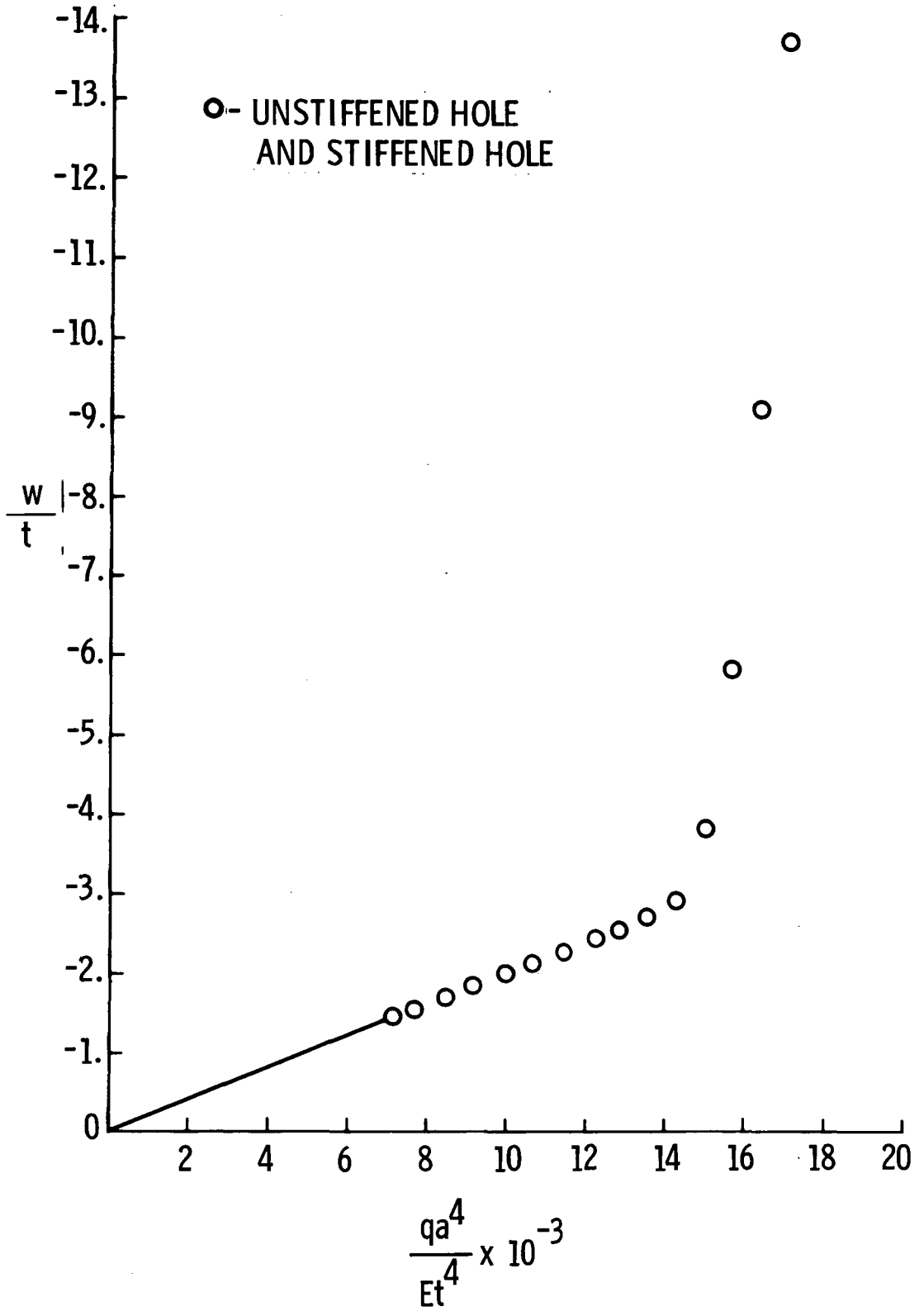

(b) NORMAL DISPLACEMENT AT r=2.5

FIG. 7 LOAD-DEFLECTION CURVES FOR RING-STIFFENED SPHERICAL SHELL UNDER EXTERNAL PRESSURE

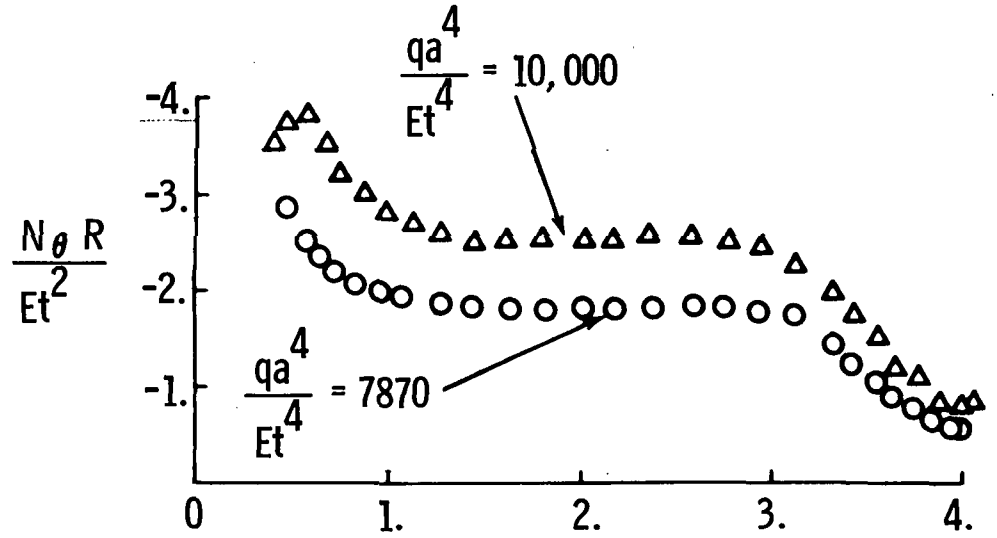

(a) DISTRIBUTION OF CIRCUMFERENTIAL STRESS RESULTANT FOR UNSTIFFENED HOLE

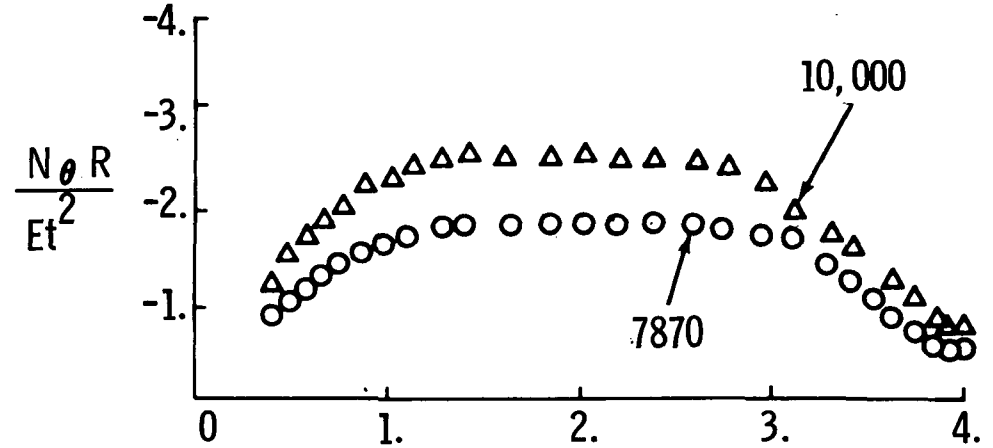

(b) DISTRIBUTION OF CIRCUMFERENTIAL STRESS RESULTANT FOR STIFFENED HOLE

FIG. 8 RING-STIFFENED SPHERICAL SHELL UNDER EXTERNAL PRESSURE

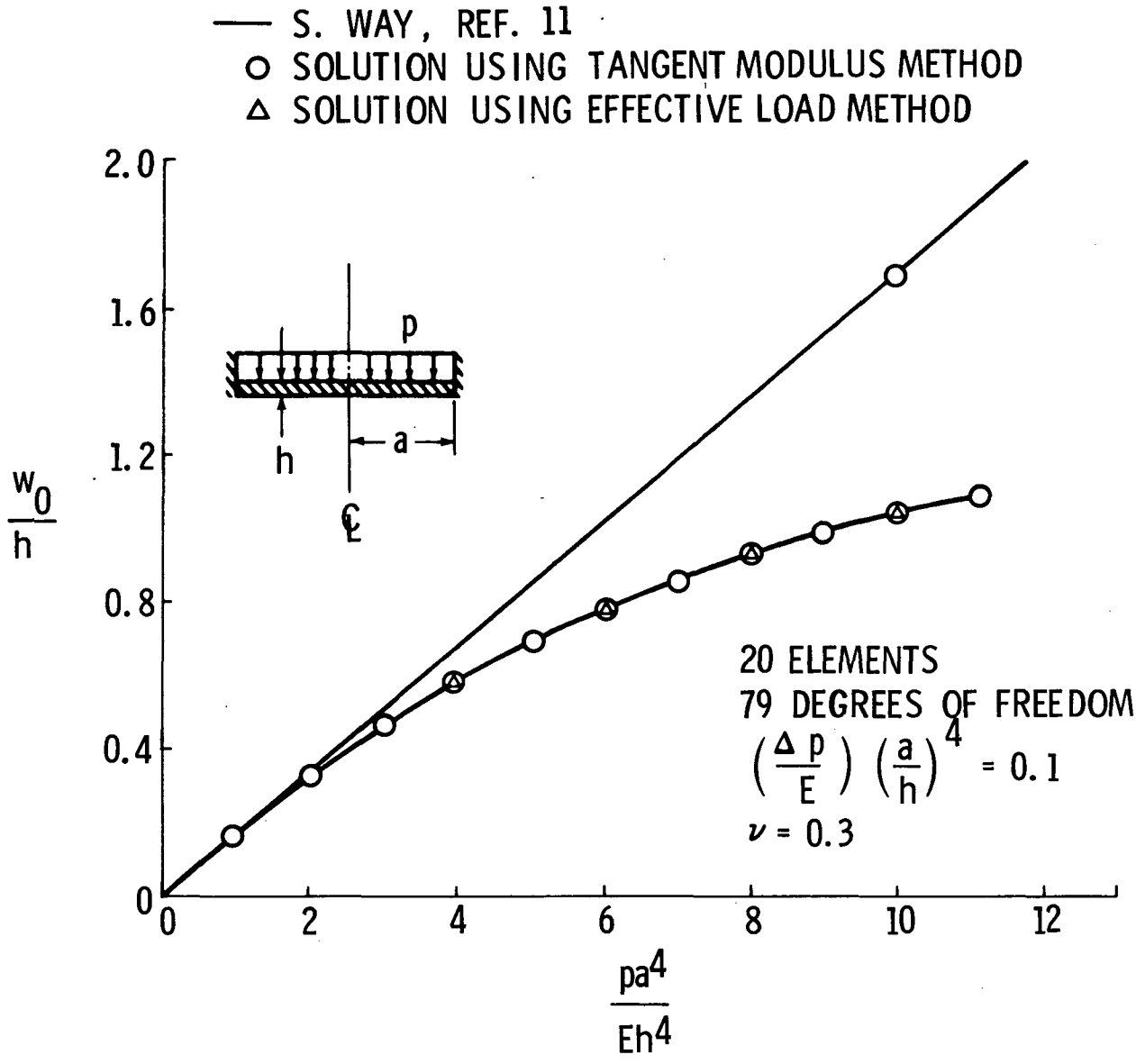

FIG. 9 CENTRAL DEFLECTION VERSUS LOAD FOR A UNIFORMLY LOADED CLAMPED CIRCULAR PLATE

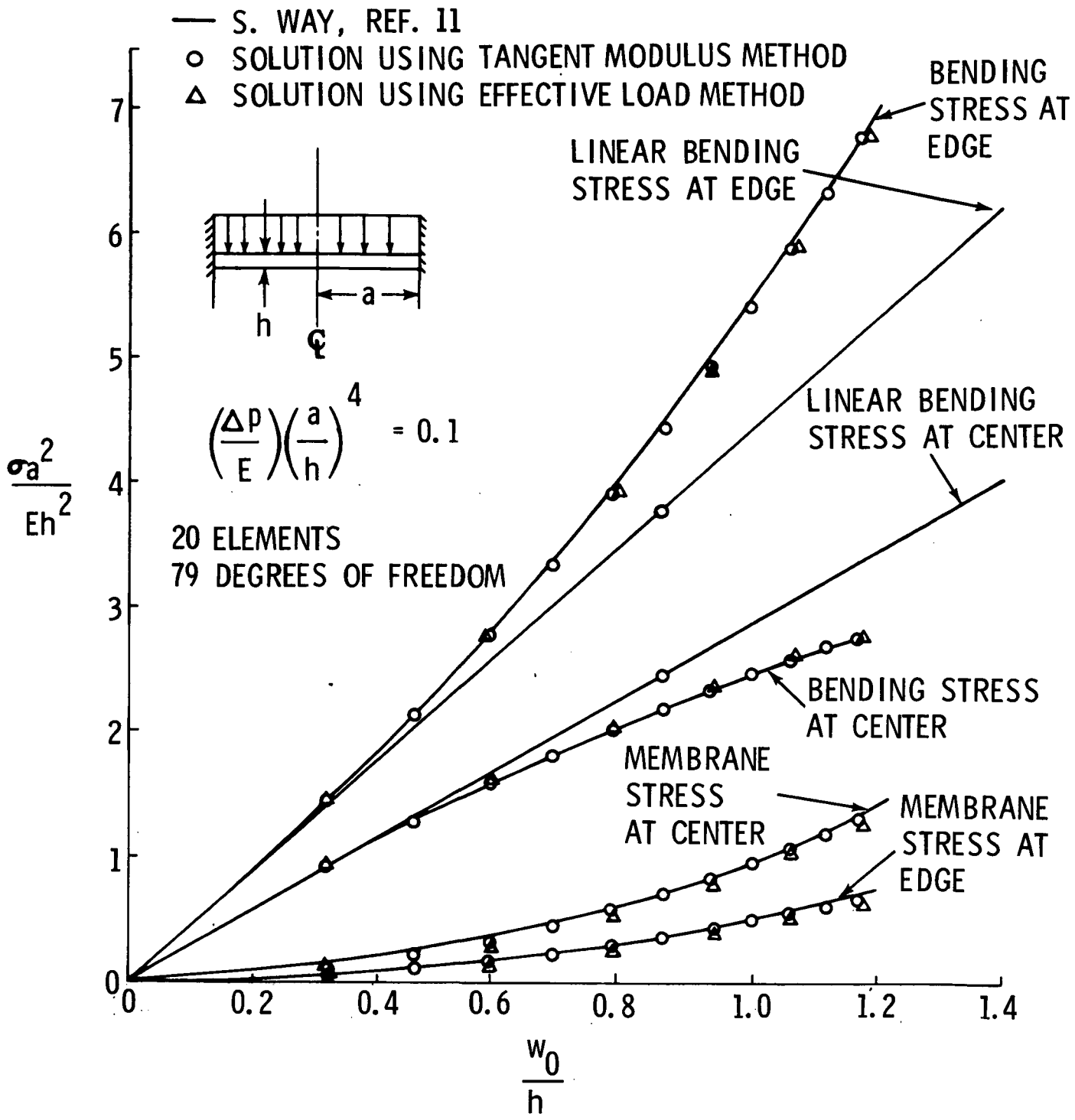

FIG. 10 STRESS VERSUS CENTRAL DEFLECTION FOR A UNIFORMLY LOADED CLAMPED CIRCULAR PLATE

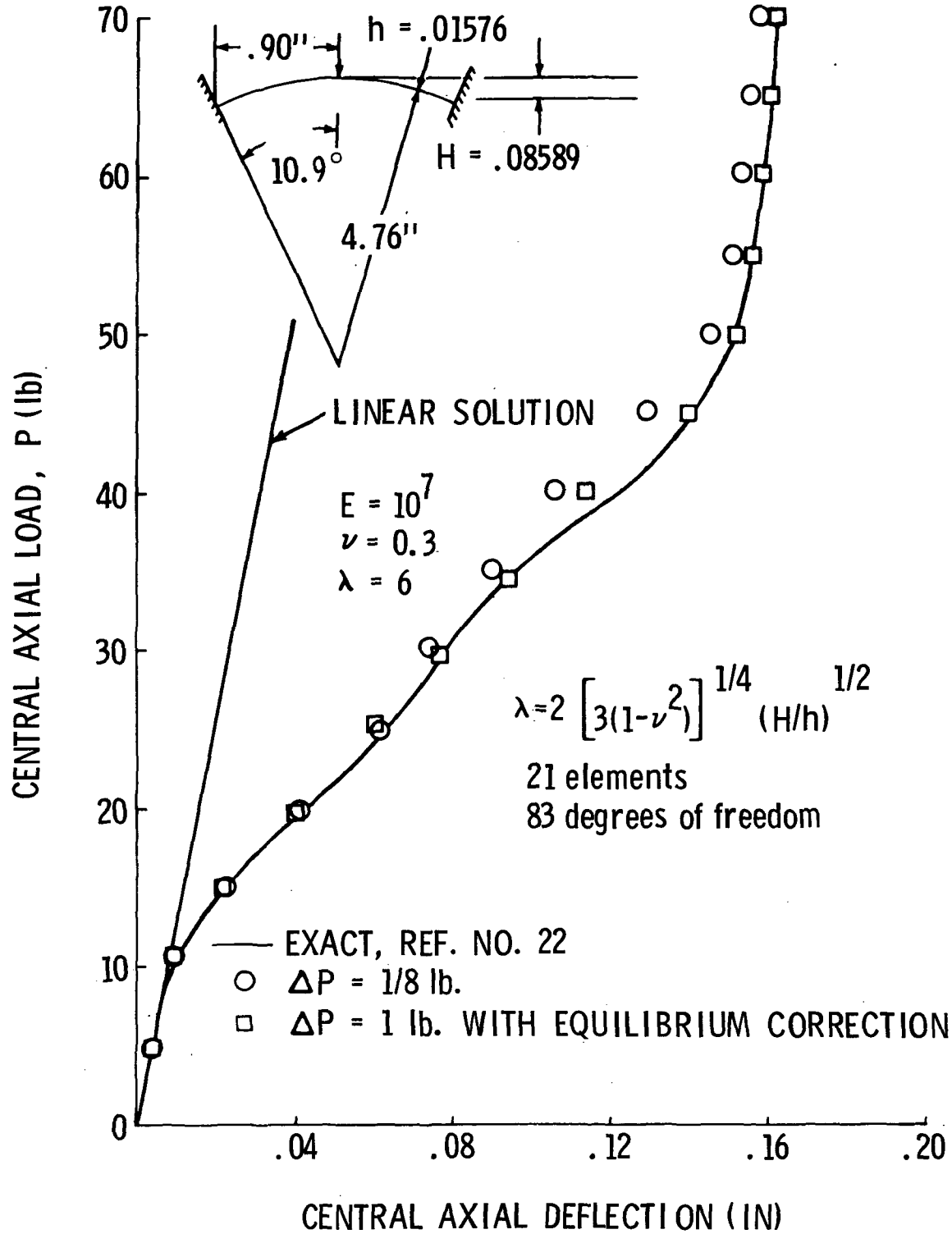

FIG. 11 LOAD VERSUS CENTRAL DEFLECTION FOR A CENTRALLY LOADED CLAMPED SPHERICAL CAP ($\lambda = 6$)

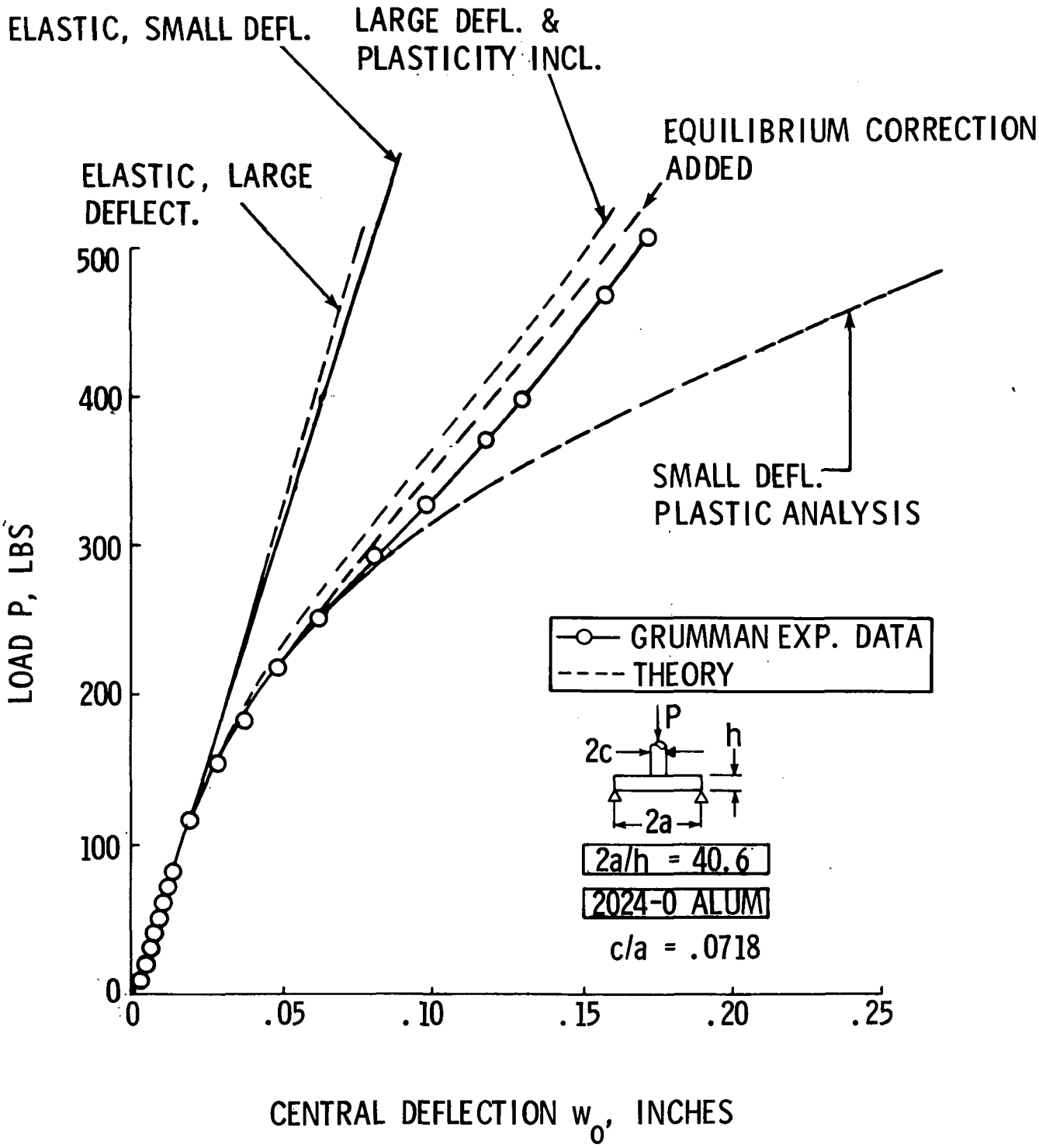

FIG. 12 LOAD VERSUS CENTER DEFLECTION FOR A SIMPLY SUPPORTED CIRCULAR PLATE (2a/h = 40.6)

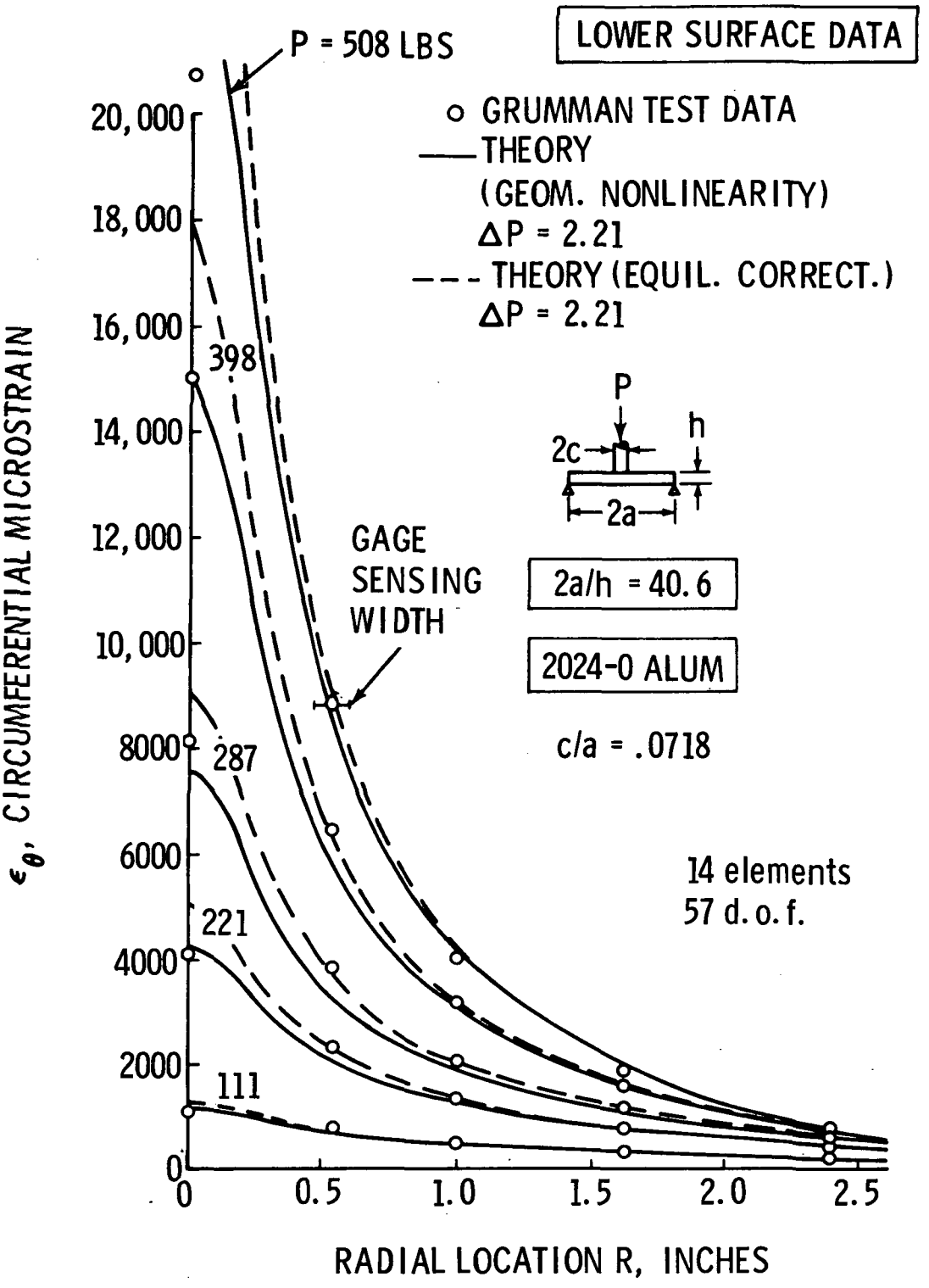

FIG. 13 CIRCUMFERENTIAL STRAIN DISTRIBUTION AT LOWER SURFACE FOR A SIMPLY SUPPORTED CIRCULAR PLATE (2a/h = 40.6)

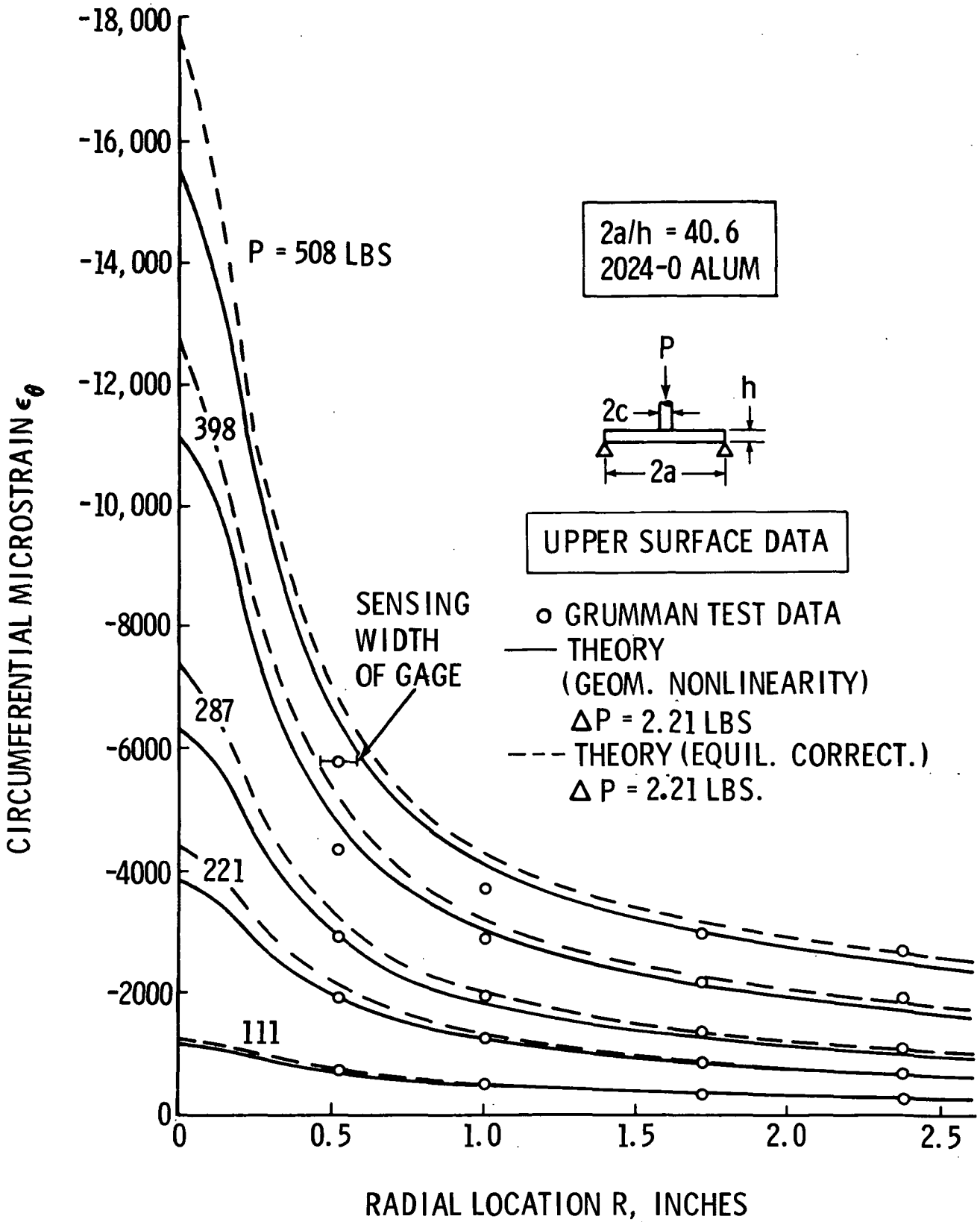

FIG. 14 CIRCUMFERENTIAL STRAIN DISTRIBUTION AT UPPER SURFACE FOR A SIMPLY SUPPORTED CIRCULAR PLATE (2a/h = 40.6)

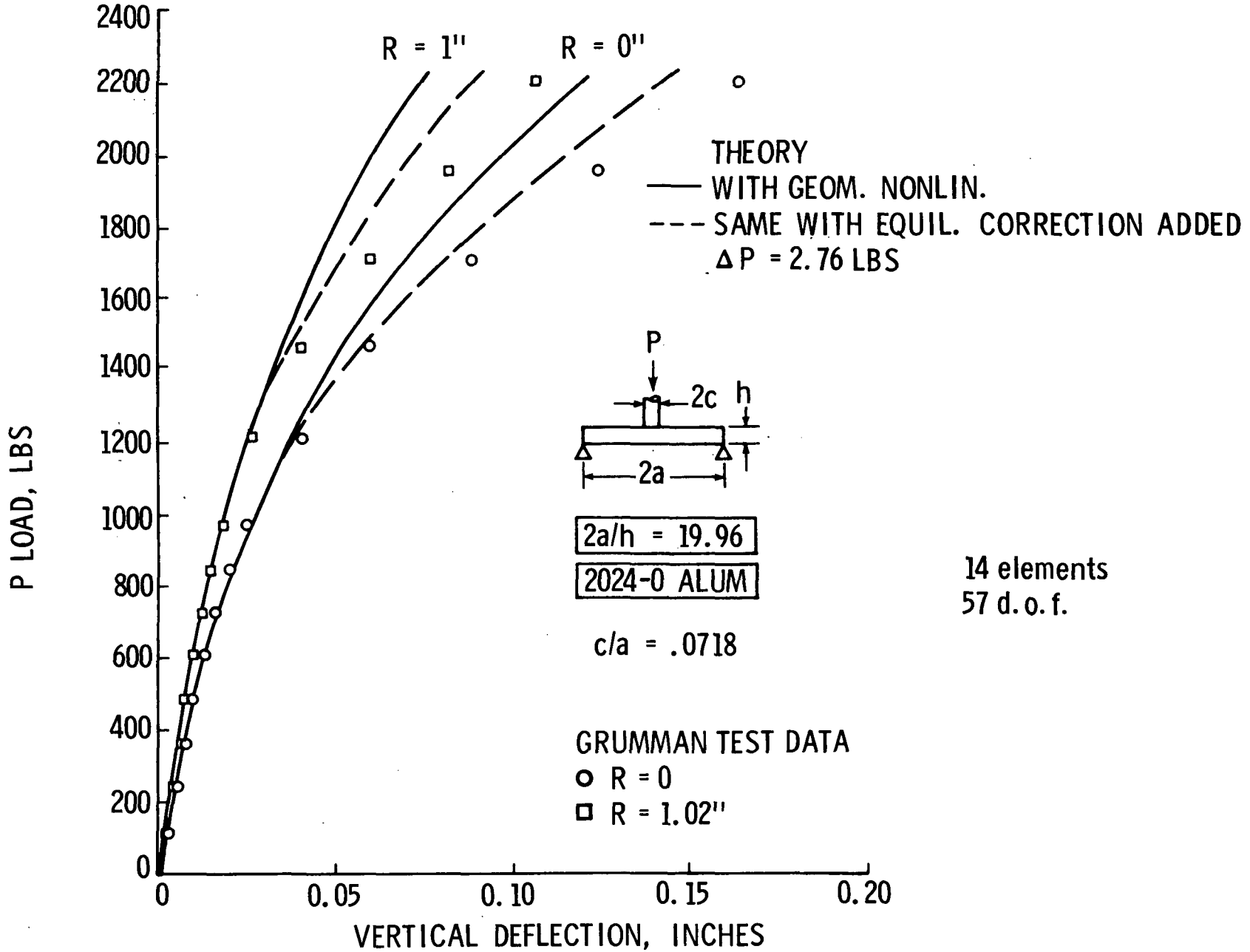

FIG. 15 LOAD VERSUS DEFLECTION FOR A SIMPLY SUPPORTED CIRCULAR PLATE (2a/h = 19.96)

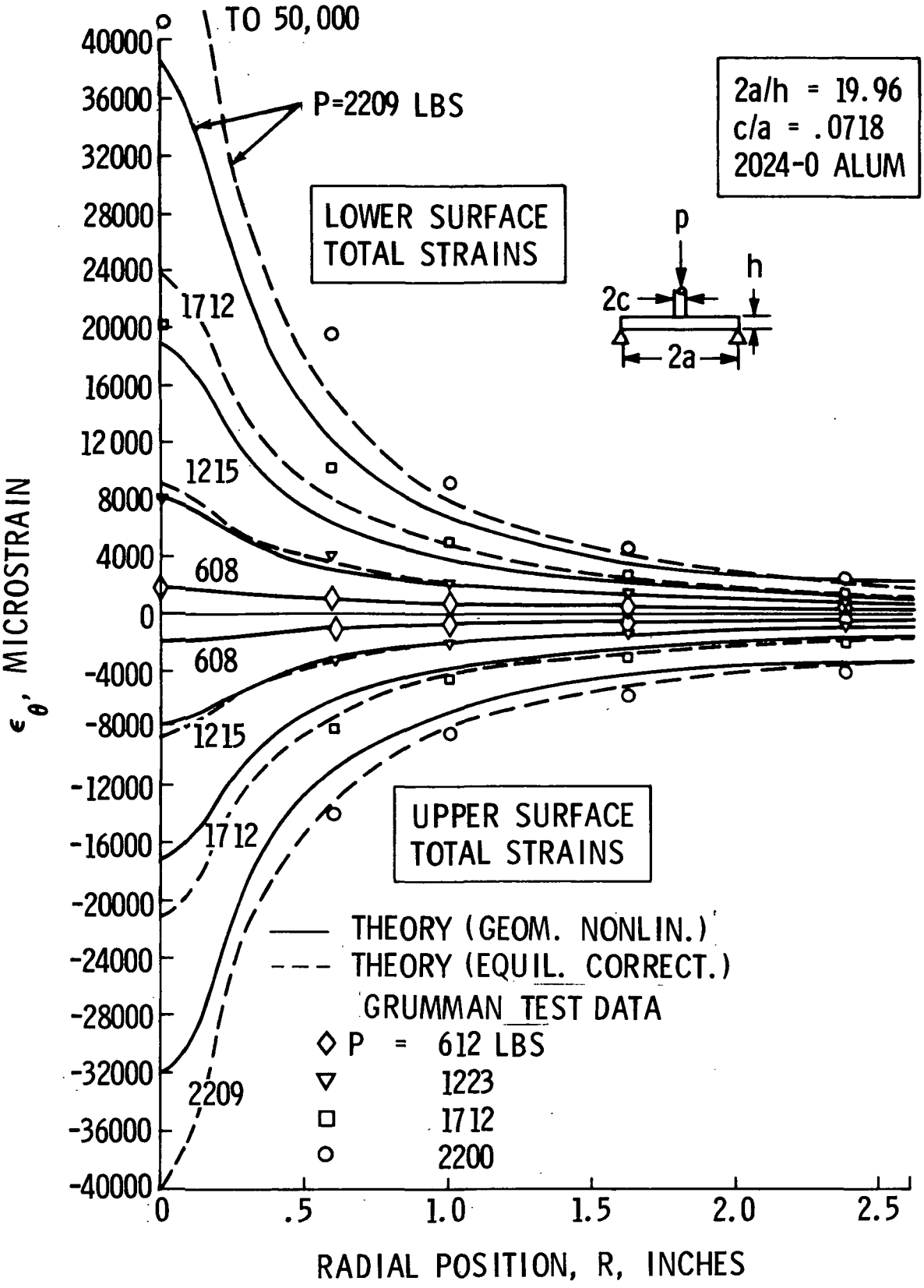

FIG. 16 CIRCUMFERENTIAL STRAIN DISTRIBUTION AT UPPER AND LOWER SURFACES FOR A SIMPLY SUPPORTED CIRCULAR PLATE (2a/h = 19.96)

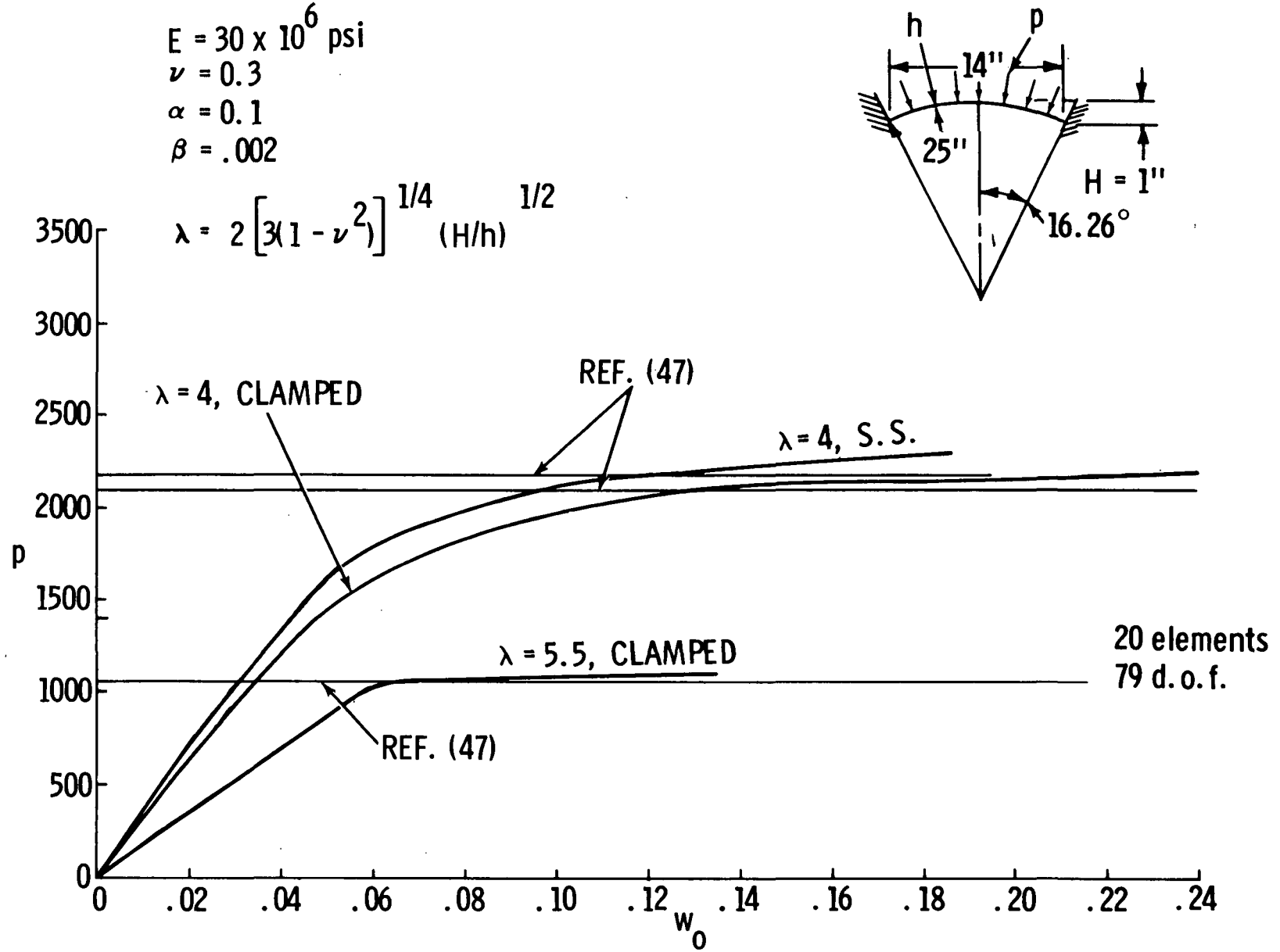

FIG. 17 ELASTO-PLASTIC BUCKLING OF SIMPLY SUPPORTED AND CLAMPED SPHERICAL CAPS UNDER UNIFORM EXTERNAL PRESSURE (LOAD VS. CENTRAL DEFLECTION CURVES)

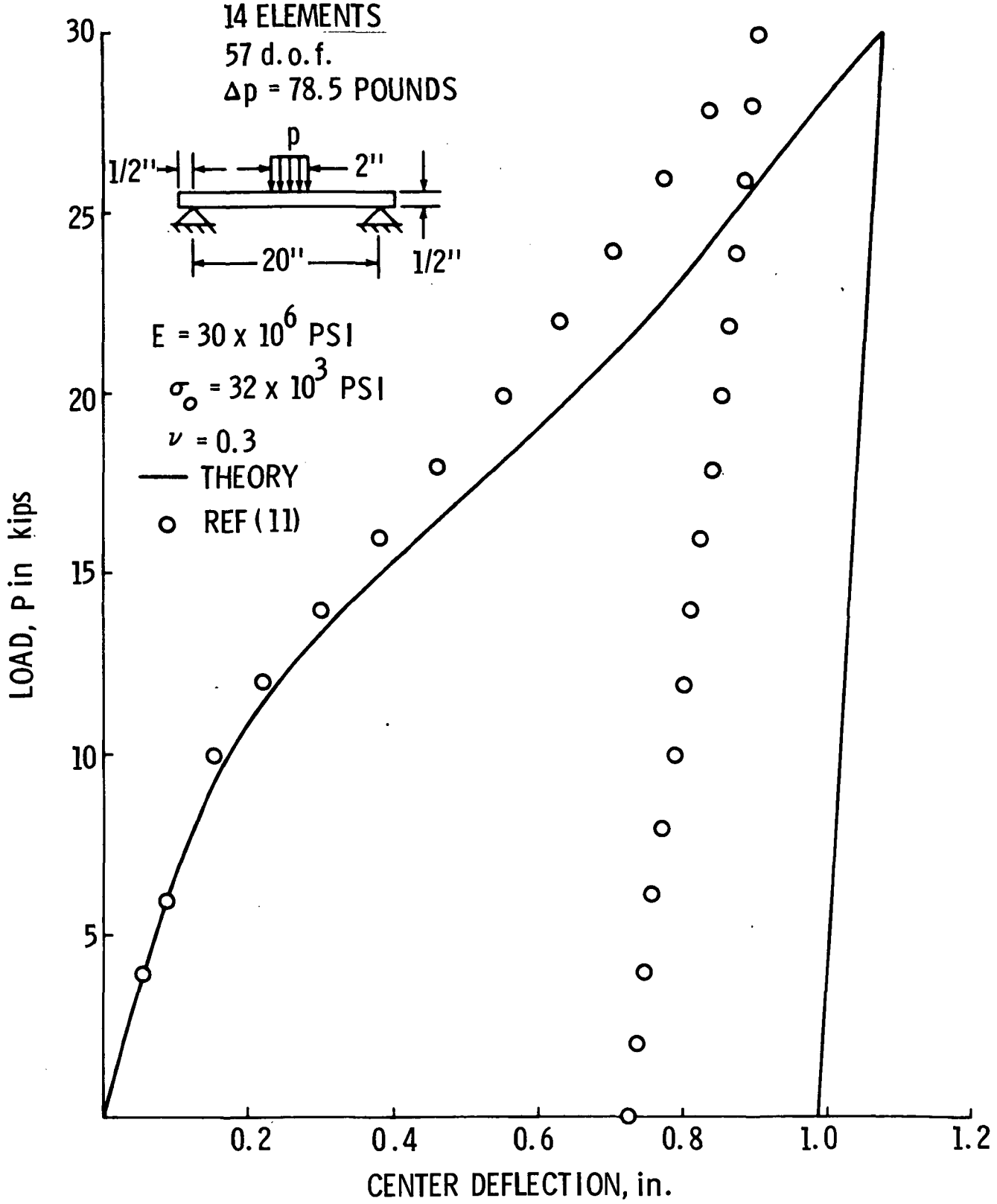

FIG. 18 LOAD VS. CENTER DEFLECTION OF A SIMPLY SUPPORTED CIRCULAR PLATE

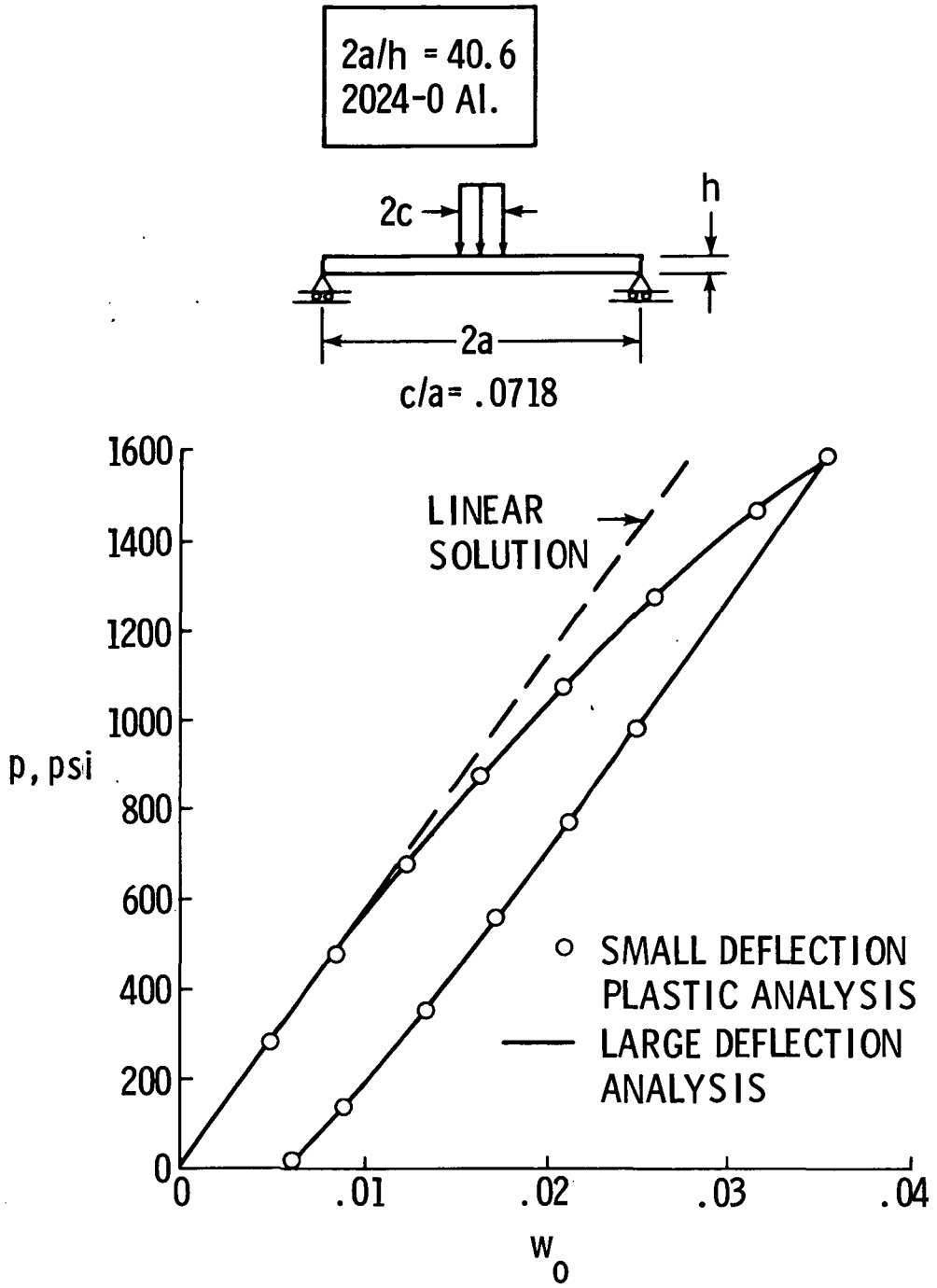

FIG. 19 HALF-CYCLE LOAD VS CENTRAL DEFLECTION FOR A SIMPLY SUPPORTED CIRCULAR PLATE (2a/h = 40.6)

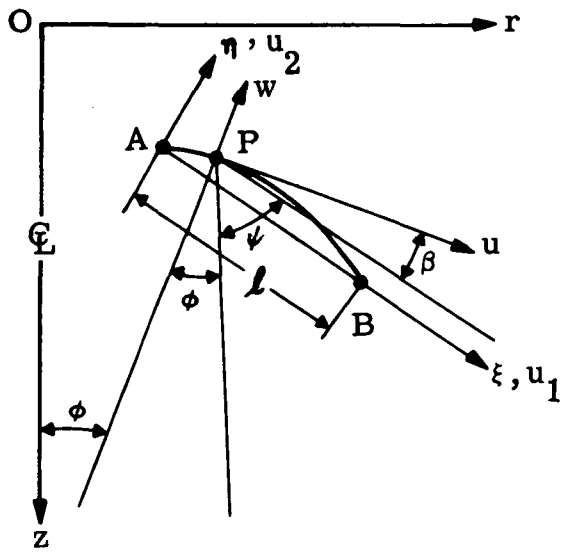

FIG. 20 DISPLACEMENTS OF THE MIDDLE SURFACE (SHELL ELEMENT)

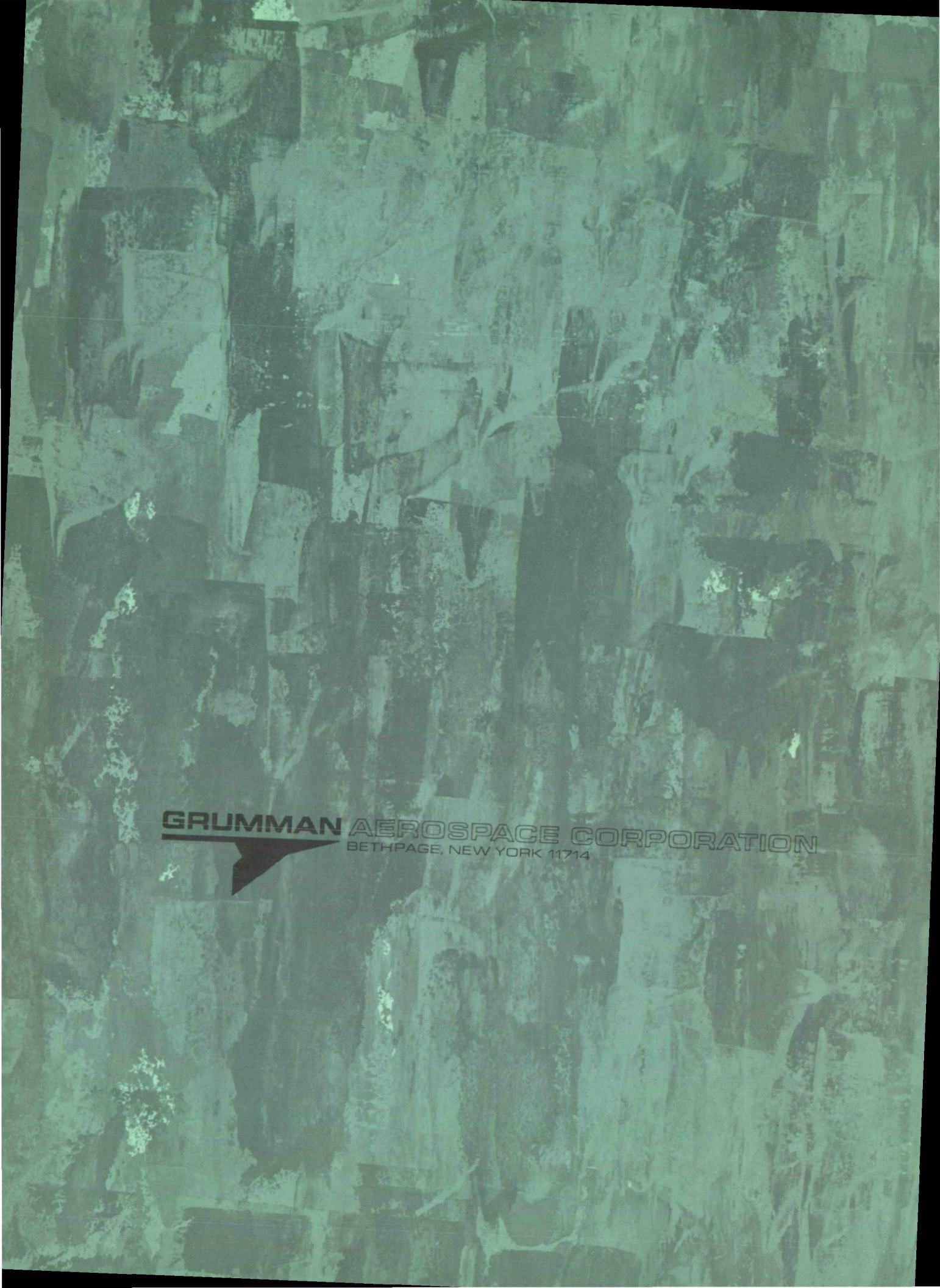
GRUMMAN AEROSPACE CORPORATION
BETHPAGE, NEW YORK 11714